

AN ABSTRACT OF THE THESIS OF

Ziwei Ke for the degree of Master of Science in Electrical and Computer Engineering presented on October 15, 2015.

Title: Low Frequency Oscillation Reduction Algorithm for Six-step Operation of Three-Phase Inverters

Abstract approved: _____

Julia Zhang

A power inverter, or inverter, is an electronic device or circuitry that converts direct currents (DC) to alternating currents (AC) in the power electronics family. A three-phase inverter converts DC current to three-phase AC current. Inverters, especially three-phase inverters, have been widely used in many fields including renewable energy applications such as interface circuits between wind turbines and the electric grid, transportation electrification such as machine drives in electric and hybrid electric vehicles, ships and aircrafts, general purpose drives for industrial applications such as pumps, fans and compressors, and the power converter circuits in medical equipment such as Magnetic Resonance Imaging (MRI) and medical power supplies.

In AC machine drive systems, the three-phase inverters can be operated by the Pulse Width Modulation (PWM) control or six-step control. With the PWM

control, the input reference voltages are modulated by a high frequency carrier wave. The top switch of the phase leg will be turned on when the reference voltage is greater than the carrier. In six-step operation control, the top switch of the phase leg will be turned on when the reference voltage is greater than zero. The advantages of using PWM control include low Total Harmonic Distortion (THD) in phase currents and controlled current. Compared to the PWM control, the six-step operation has advantages containing reduced switching losses, better utilization of DC bus voltage, and extended speed capability.

In analog implementation of the six-step control, the control signals of the switches are generated by a comparator in the electronic circuit. Hence, the switches will be turned on and off at the phase voltage zero crossing points. In digital implementation, however, power electronics may not be able to switch on and off exactly at the zero crossing points of the phase voltage due to the limited resolution of the sampled phase voltage command, which will result in a DC offset in the phase voltage and cause a low frequency oscillation in the phase current. The low frequency oscillation will create issues such as higher power loss, lower efficiency, and excessive heat that may permanently demagnetize permanent magnets on the rotor for a permanent magnet (PM) synchronous machine.

This research investigates a control method to significantly reduce the low frequency oscillation phase current for the six step operation of a three-phase inverter in digital implementation. The proposed control method using asymmetric PWM ensures that power electronics switch on and off exactly at the voltage zero crossing points. The algorithm calculates the duty ratio when the phase voltage command

crosses zero from positive to negative or from negative to positive. In addition, the control algorithm was simulated and tested on a three-phase RL load and a PM synchronous machine. Both simulation and experimental results demonstrate that the proposed control algorithm can reduce the low frequency oscillation components in the phase current by more than 90%.

©Copyright by Ziwei Ke
October 15, 2015
All Rights Reserved

Low Frequency Oscillation Reduction Algorithm for Six-step
Operation of Three-Phase Inverters

by

Ziwei Ke

A THESIS

submitted to

Oregon State University

in partial fulfillment of
the requirements for the
degree of

Master of Science

Presented October 15, 2015
Commencement June 2016

Master of Science thesis of Ziwei Ke presented on October 15, 2015.

APPROVED:

Major Professor, representing Electrical and Computer Engineering

Director of the School of Electrical Engineering and Computer Science

Dean of the Graduate School

I understand that my thesis will become part of the permanent collection of Oregon State University libraries. My signature below authorizes release of my thesis to any reader upon request.

Ziwei Ke, Author

ACKNOWLEDGEMENTS

I would like to express my sincere gratitude to a number of people who have helped me throughout my research. First and foremost, I am grateful to my advisor, Dr. Julia Zhang, for providing tremendous levels of support over the last two years. Her mentoring, encouragement and persistence have shaped my own engineering problem-solving approach. Her profound knowledge, hard working and enormous experience in research, and great patience in teaching inspired me and helped me to gradually develop critical thinking. It has been a sincere privilege to study under her direction.

I would also like to thank Dr. Eduardo Cotilla-Sanchez, Dr. Ted Brekken and Dr. Annette von Jouanne, for considerable useful discussions, ideas and advice especially when we were working on the BPA project together, which all contributed to my graduate study at OSU. Their help and advice allowed me to excel much more than I ever could have alone.

I would also like to acknowledge Dr. Raviv Raich, who gave me great ideas and suggestions on the data analysis of this research work.

Thanks are due to my committee, Dr. John Parmigiani, Dr. Eduardo Cotilla-Sanchez, Dr. Ted Brekken, and Dr. Julia Zhang, for their involvement, feedback and the time that they spent reviewing this thesis.

As a student of the energy system research group, my fellow group members and officemates in the Dearborn basement and Kelley Engineering Building have made my graduate school experience better in many ways. I would like to thank my

senior fellow student Lei Jin for his help, useful discussions and instructions on this research work. I would also like to thank Ben McCamish, Scott Harpool, Janhavi Kulkarni, Chen Huo, and Dr. Jiajia Song for their help in the BPA project. I also want to thank Han Xiong, Ratanak So, Michael Starrett, Alex Louie, Ridwan Azam, Asher Simmons and Qianyun Li for their friendship.

Lastly I would like to thank my parents and my family in China for their continued support and unconditional love. All the support they have provided me over the years was the greatest gift anyone has ever given me. Without their support and love, I can't study and finish my Master degree here at OSU.

TABLE OF CONTENTS

	<u>Page</u>
1 Introduction	1
1.1 Power Inverters	1
1.2 AC Machine Drive Control Systems	4
1.2.1 PWM Control	6
1.2.2 Six-step Operation Control	9
1.3 Motivations of this work	11
1.4 Literature Review	13
1.5 Chapter Review	15
2 Low Frequency Harmonic Production Mechanism and Principle of Low Frequency Harmonic Reduction Algorithm	17
2.1 Principle of Analog PWM Signals Generation	17
2.2 Digital Implementation of PWM Algorithm	18
2.3 Principle of Low Frequency Harmonic Production	22
2.4 Principle of Low Frequency Harmonic Reduction Algorithm	25
2.5 Dead-time Effect and Short Pulse Elimination	28
3 Mathematical Modeling and Control Algorithms of PM Synchronous Machines	32
3.1 Reference Frame Transformation Theory	32
3.2 Mathematical Modeling in Rotating Reference Frame and Torque Equations of PM Machines	36
3.3 PWM Control	38
3.4 Six-step Control	40
4 Simulation Verification	44
4.1 Simulation Results of RL load	44
4.2 Simulation Results of Interior Permanent Magnet Synchronous Machine Load	48

TABLE OF CONTENTS (Continued)

	<u>Page</u>
5 Experimental Verification	54
5.1 Experimental Results using RL load	54
5.1.1 Experimental Results at $f_s = 8kHz$ & $f_1 = 1100Hz$	56
5.1.2 Experimental Results at $f_s = 8kHz$ & $f_1 = 1700Hz$	58
5.2 Experimental Results using Interior Permanent Magnet Synchronous Machine Load	60
6 Conclusions and Future Work	66
6.1 Summary and Conclusions	66
6.2 Future Work	68
Bibliography	69

LIST OF FIGURES

<u>Figure</u>	<u>Page</u>
1.1 Single phase inverter of two major topologies	3
1.2 Typical configuration of modern AC machine drive systems	4
1.3 Three-phase voltage source power inverter	5
1.4 Fundamental principle of voltage second balance	7
1.5 PWM signals with different duty ratios	8
1.6 Switching signal of top switch of one phase leg in PWM control without over-modulation	9
1.7 Switching signal of top switch of one phase leg in six-step operation	10
1.8 Voltage waveforms in six-step operation	10
1.9 Voltage zero crossing points	12
1.10 Phase current with obvious low frequency oscillation	13
2.1 PWM signal waveform terms	19
2.2 PWM signal waveform terms and counter wave	20
2.3 Digital implementation of PWM	21
2.4 Digital sampling methods	23
2.5 Principle of low frequency harmonic production	24
2.6 Low frequency harmonic reduction algorithm of Case I & II	27
2.7 Dead time configuration	28
2.8 Switching signal with dead time configuration	29
2.9 Configuration options for the dead-band submodule	30
2.10 Dead-band waveforms	30
2.11 Short pulses elimination	31

LIST OF FIGURES (Continued)

<u>Figure</u>	<u>Page</u>
3.1 Combined several reference frames	33
3.2 Block diagram speed closed-loop SVPWM control of PM synchronous machine	39
3.3 Block diagram speed closed-loop voltage phase angle control in six-step operation of PM synchronous machine	40
3.4 Definition of V_s and θ_v	41
3.5 Voltage vector in $d-q$ and abc reference frame	43
4.1 Schematic of simulation system using RL load	45
4.2 Simulation results: switching signals and current of Phase A without using low frequency harmonic reduction algorithm	46
4.3 Simulation results: switching signal and three-phase current applying low frequency harmonic reduction algorithm	47
4.4 Simulation results: spectrum analysis of Phase A current before and after applying low frequency harmonic reduction algorithm	48
4.5 Schematic of simulation system using machine load	49
4.6 Simulation results: Phase currents I_a & I_b , and line-to-line voltage V_{ab} before and after applying the low frequency harmonic reduction algorithm	52
4.7 Spectrum analysis of Phase A current before and after applying low frequency harmonic reduction algorithm	53
5.1 Hardware testing system using RL load	55
5.2 Experimental results: three-phase switching signals without applying low frequency harmonic reduction algorithm	56
5.3 Experimental results: currents of Phase A and B before and after applying low frequency harmonic reduction algorithm	57

LIST OF FIGURES (Continued)

<u>Figure</u>	<u>Page</u>
5.4 Experimental results: spectrum analysis of Phase A current before and after applying low frequency harmonic reduction algorithm . . .	58
5.5 Experimental results: currents of Phase A and B before and after applying low frequency harmonic reduction algorithm	59
5.6 Experimental results: spectrum analysis of Phase A current before and after applying low frequency harmonic reduction algorithm . . .	60
5.7 Experimental results: Phase currents I_a & I_b , line-to-line voltage V_{ab} , and zoom-in line-to-line voltage V_{ab} before applying the low frequency harmonic reduction algorithm	63
5.8 Experimental results: Phase currents I_a & I_b , line-to-line voltage V_{ab} , and zoom-in line-to-line voltage V_{ab} after applying the low frequency harmonic reduction algorithm	64
5.9 Spectrum analysis of Phase A current before and after applying low frequency harmonic reduction algorithm	65

LIST OF TABLES

<u>Table</u>		<u>Page</u>
4.1	Ratings and parameters of the PM machine	49

Chapter 1: Introduction

This chapter provides a general introduction to power inverters and AC electric machine drive systems using pulse width modulation (PWM) control and six-step operation control. In addition, motivations of this work, literature review and chapter review in this thesis are summarized.

1.1 Power Inverters

Power electronics is the application of solid-state electronics to control and convert electric power. Power electronic devices provide an interface between electric circuitries or systems, such as connection of two asynchronous alternating current (AC) systems or conversion from AC to direct current (DC) and vice versa. Due to the advancements of the circuitry topologies of the power converters and the strong growth of the material technology of power semiconductors, power electronic systems are now more efficient and reliable, and have a higher power density with smaller size and weight.

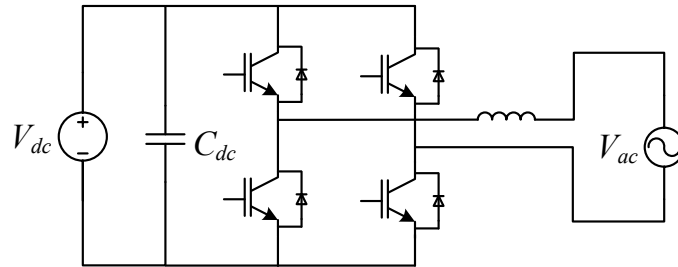
Power converters are used to convert electric power by using power electronic devices. In general, power converters can be classified into 4 different types according to whether their inputs and outputs are AC or DC. These 4 different types are DC-DC, AC-DC, AC-AC and DC-AC converters. For example, DC-DC con-

verters include buck and boost converters. Rectifiers and inverters are the typical devices of AC-DC converters and DC-AC converters respectively. Transformers and cycloconverters are AC-AC converters.

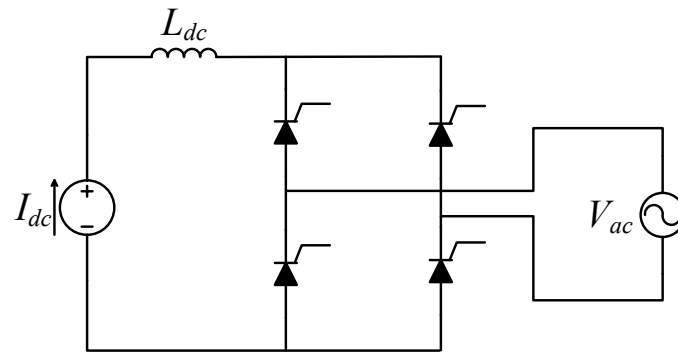
A power inverter is a converter that converts power from DC to AC. Power inverters usually have the bi-directional functionality and the AC output could be a variable frequency and variable voltage magnitude system depending on the design of the specific device or the circuitry. Power Inverters are used in our lives including commercial applications such as hybrid electric vehicles, air-conditioning power supplies, computers and elevators; residential applications such as cell phone chargers, washing machines and dryers; industrial applications such as blowers, fans, pumps, compressors, wind turbines and wave energy converters.

According to the input source type, inverters can be divided into voltage-source inverters (VSIs) and current-source inverters (CSIs). Figure 1.1(a) shows the VSI topology of a single phase inverter. The single-phase CSI topology is shown in Figure 1.1(b). The single-phase inverter operates in two different statuses by turning on and off the switches alternately. The output voltage is either equal to the positive dc bus voltage or negative dc bus voltage.

VSIs are prominent in the commercial markets since VSIs have proven to be more efficient, and have higher reliability and faster dynamic responses. Furthermore, the VSI topology design costs less with higher efficiencies and minimizes the install time. CSIs are still utilized in applications with extremely high power levels where thyristor-based switches are still popular [1]. According to Reed, one reason of the successes of the CSI topology was that its property was well-aligned with



(a) Single phase voltage source inverter



(b) Single phase current source inverter

Figure 1.1: Single phase inverter of two major topologies

the strengths of the switching devices available at the time [2]. Due to the limited applications, the CSIs are not discussed in this research.

The VSIs can be further divided into the three general categories including PWM inverters, Square-wave inverters and single-phase inverters with voltage cancellation.

The PWM inverters control the magnitude and the frequency of the AC output voltages by using PWM technique. There are several PWM schemes to shape the output AC voltages to be as close to a sine wave as possible. Details of the PWM inverter will be discussed in this chapter and chapter 2.

For the square-wave inverters, the output AC voltage has a waveform similar

to a square wave. The input dc voltage is controlled in order to control the magnitude of the output AC voltage, and therefore the inverter has to control only the frequency of the output voltage.

The single-phase inverters with voltage cancellation combine the characteristics of the previous two inverters. The magnitude and the frequency of the inverter output voltage can be controlled and the output voltage waveshape is square wave.

Furthermore, based on the number of phases of the output AC signals, the inverters can be classified into single-phase inverters and three-phase inverters.

1.2 AC Machine Drive Control Systems

An AC machine drive system consists of the following components as shown in Figure 1.2: a controller, a power inverter, an AC machine and feedback transducers or sensors that convert current, voltage, position and speed signals [3].

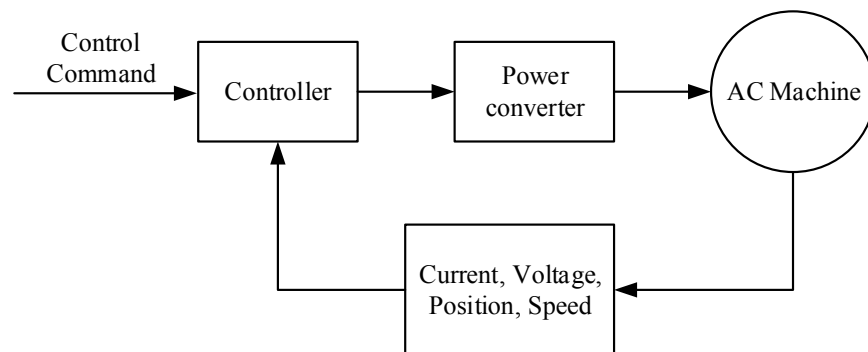


Figure 1.2: Typical configuration of modern AC machine drive systems

In response to an input control command, electric drives efficiently control the speed and the position of the machine. The controller, by comparing the

control command for speed and position with the actual feedback values measured through sensors, provides appropriate control signals to the power converter. A digital signal processor (DSP) is commonly used as a controller. By receiving the control signals, the power converter converts the power from DC to AC to power the AC machine. The AC machine can be an induction machine or a synchronous machine. The transducers or sensors measure the status of the machine and provide voltage, current, rotor position and speed to the controller. Microprocessors with fast computation performance and modern control theories have made it possible to control these AC electric machines as convenient as DC machines [4].

A three-phase inverter is used to power the AC machine. Figure 1.3 demonstrates a three-phase inverter using the VSI topology. V_{dc} is the input voltage source. In each phase leg, the switching signals of the top and the bottom switches are complemented. Both of them can not be turned on at the same time. Otherwise, it will cause short circuit and damage the devices. The gate signals of these six switches are generated by the controller. Variable frequency and variable voltage magnitude of the AC output can be achieved by using the PWM control technology.

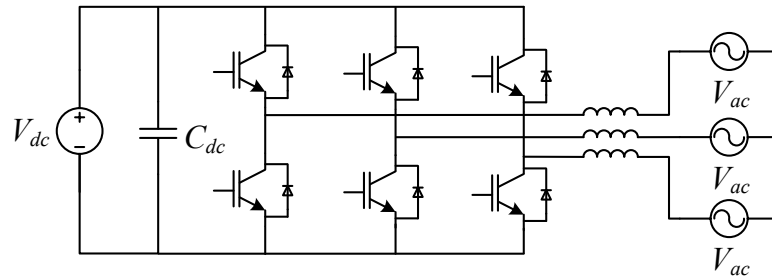


Figure 1.3: Three-phase voltage source power inverter

1.2.1 PWM Control

The PWM modulation technique aims to create trains of switched pulses which have the same fundamental volt-second balance as a target reference waveform. Figure 1.4 shows the fundamental principle of the voltage second balance. The triangle waveform is the carrier wave. Since the frequency of the carrier is much higher than the phase voltage command, the magnitude of the reference voltage is assumed as a constant value in one cycle of the carrier. The bottom waveform is the output voltage of a single phase inverter. In order to achieve an equivalent performance as the input reference voltage for the output voltage, the integral of the reference voltage should be equal to the integral of the output voltage over one switching cycle of the carrier. In other words, Area A is equal to the sum of Area 1 and Area 3 minus Area 2 in the figure.

The PWM modulation technique is a principle algorithm that is widely used in power electronics and electric machine drive systems. A PWM signal consists of two major parameters: a duty cycle and a frequency. A duty cycle, also called duty ratio, describes the percentages of time that a switch is turning on during one switching cycle. The duty ratio should be a number between 0 and 1. The frequency defines how fast the next pulsing signals are generated. Figure 1.5 shows three PWM signals with 20%, 50% and 80% duty cycles from the top to the bottom respectively. T_s is the switching cycle.

In real-world applications, the duty cycle could be a constant value or a changing variable. It depends on the control commands from the controller for different

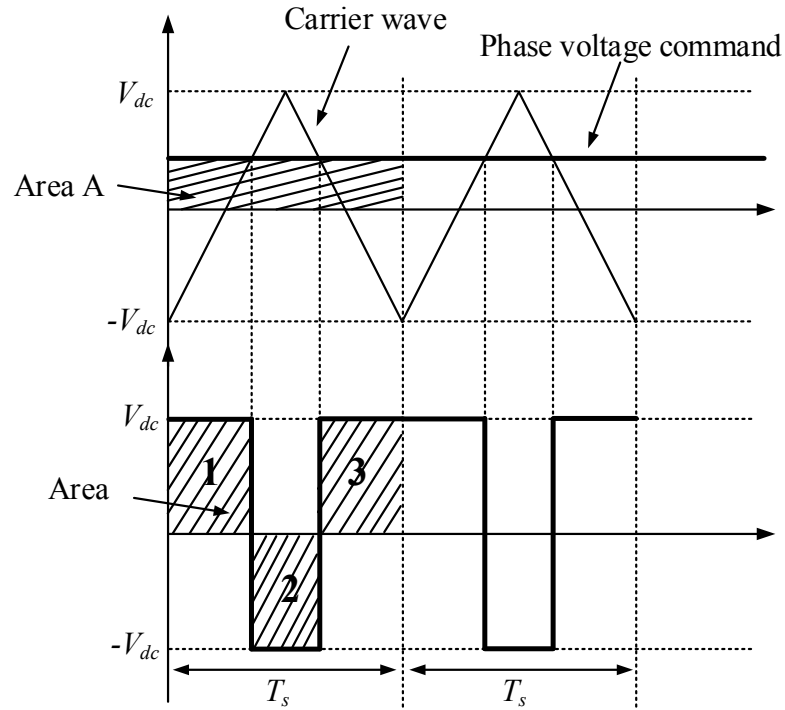


Figure 1.4: Fundamental principle of voltage second balance

purposes. In electric machine drive systems, a PWM signal can be produced using analog or digital methods. In analog, a command signal is compared with a triangular carrier wave to determine the output PWM signals; while in digital, the duty ratio will be calculated in advance to generate the PWM signals.

Figure 1.6 shows the PWM implementation in AC machine drive systems. The phase voltage command compares with the carrier wave to generate PWM signals. Typically, the carrier is represented by a triangular wave. The frequency of the phase voltage command is the fundamental frequency f_1 and the frequency of the carrier wave is equal to the switching frequency f_s . Hence, the frequency of the PWM signal is also equal to the switching frequency f_s . An “On” signal will be

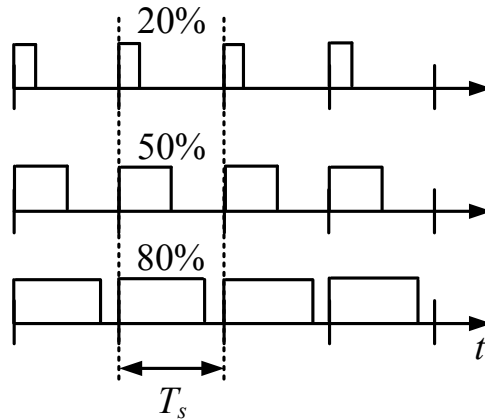


Figure 1.5: PWM signals with different duty ratios

generated when the phase voltage command is greater than the carrier; while an “Off” signal is generated if the phase voltage command is less than the carrier. The output PWM waveforms will be converted to actual gate signals, that turn on or off the switches of the inverter. Variable frequency and variable voltage magnitude of the AC output can be achieved by modifying the frequency and magnitude of the phase voltage command.

Volts per hertz control, field oriented control and direct torque control are widely developed and used in PM synchronous machines, whose excitation fields are provided by a permanent magnet instead of a coil. Regardless of which control method is applied, the PWM control technique is used to drive the inverter to power the machine.

The advantages of using PWM control include low total harmonic distortion (THD) and controlled current. However, a high switching frequency generally at least ten times higher than the fundamental frequency of the electric machine

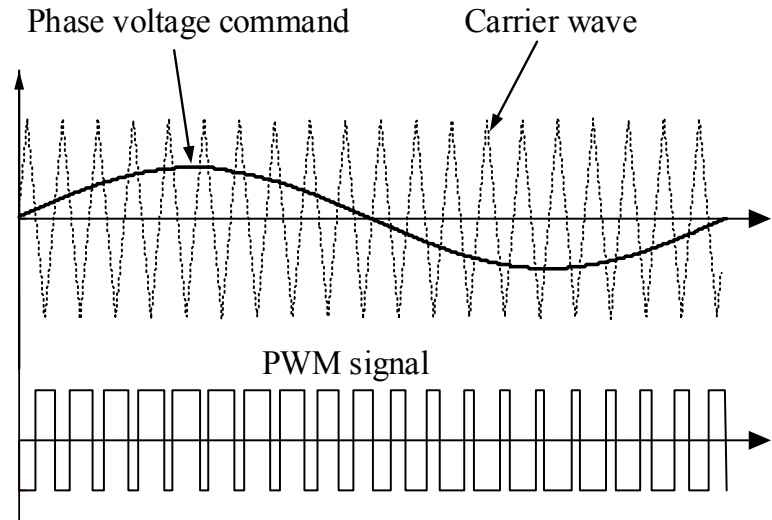


Figure 1.6: Switching signal of top switch of one phase leg in PWM control without over-modulation

is required to ensure a sinusoidal phase current with low THD [5]. For a high fundamental frequency, fewer pulses are created for each fundamental cycle if the switching frequency is fixed, which increases the total harmonic distortion. When the electric machine operates at a high speed, the six-step control is applied.

1.2.2 Six-step Operation Control

The fundamental principles of six-step operation are demonstrated by Figure 1.7 and 1.8. Figure 1.7 shows the switching signal of the top switch in one of the phase legs of the power inverter when six-step control is operated. The top switch of that phase will be turned on when the reference voltage is larger than zero, and it will be turned off when the reference voltage is less than zero. The turn-on time and the turn-off time are identical to each other.

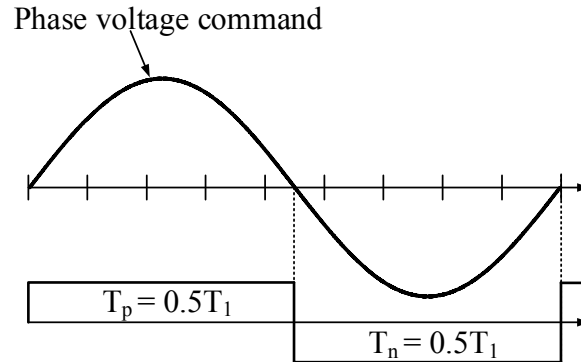


Figure 1.7: Switching signal of top switch of one phase leg in six-step operation

Figure 1.8 shows the output voltage waveforms of a three-phase inverter in six-step operation. The top waveform is the line-to-line voltage V_{ab} , whose peak value is the dc bus input voltage. The bottom three waveforms are the phase-to-neutral voltages V_a , V_b and V_c with 120° apart. In addition, the shape of the voltage waveform has six different levels in one fundamental cycle, which contributes to the origin of the name of six-step.

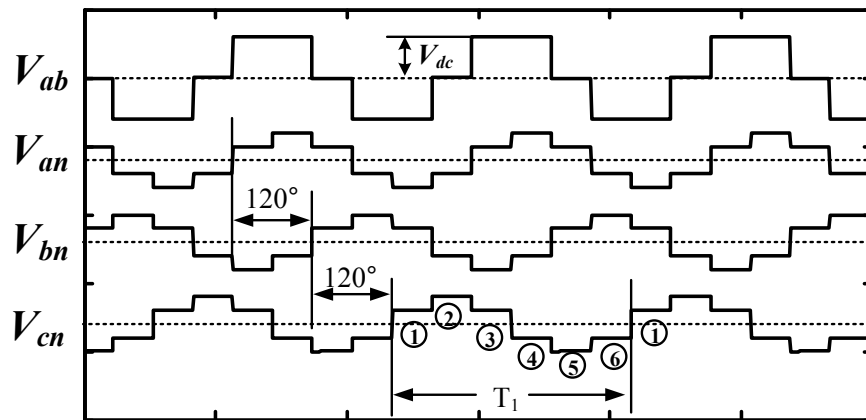


Figure 1.8: Voltage waveforms in six-step operation

The six-step operation is often applied to reduce the power electronics switch-

ing loss and expand the machine speed capability [6]. In addition, the fundamental components of the output voltages are also maximized. The output voltage could be enhanced by 10.27% compared to space vector PWM by applying six-step operation [7]. The fundamental harmonic of the phase voltage reaches the theoretical maximum of $\frac{2}{\pi}V_{dc}$ when it operates in six-step mode. Therefore, the torque capability and operation region of PM synchronous machines can be extended. However, phase currents can't be controlled in six-step operation and lower order harmonic currents will be introduced, which cause additional iron losses. In addition, it generates high torque ripple and acoustic noise.

1.3 Motivations of this work

In analog implementation of the six-step control, the control signals of the switches are generated by a comparator in the electronic circuit. Hence, the switches will be turned on and off exactly at the phase voltage zero crossing points. As shown in the figure 1.6, however, the ratio $m_f = f_s/f_1$ between the switching frequency f_s and the electrical fundamental frequency f_1 , or called the carrier-fundamental frequency ratio, might not be an integer in digital control. Power electronics may not be able to switch on or off exactly at the voltage zero crossing points when the frequency ratio is a non-integer number. Figure 1.9 shows the reference voltage and the sampling points. If the frequency ratio m_f is not an integer. The voltage zero crossing points (Red dots) are between the sampling points. This will create a DC offset in the phase voltage over one fundamental cycle, hence, a low frequency

oscillation in the phase current.

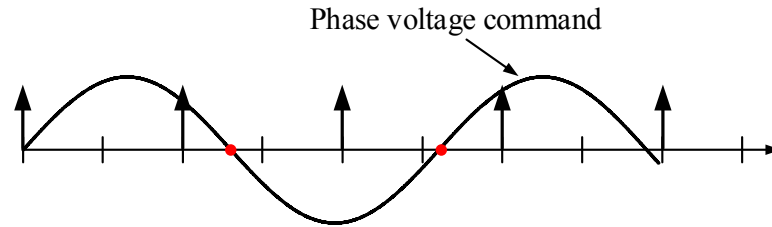


Figure 1.9: Voltage zero crossing points

Figure 1.10 shows one phase current of a three-phase inductance load using the six-step control. The fundamental and switching frequencies are 0.7 kHz and 5 kHz. The dash curve shows the low frequency harmonic component. The low frequency oscillation in the phase current is harmful to the whole electric machine drive system in multiple ways. Firstly, the subharmonic current will appear as unnecessary power flow between the electric machine and the source. This will generate extra copper losses in every stage of the electric machine drive system - the source, power converters and the electric machine - resulting in an overall reduction in the system efficiency. Secondly, the low frequency harmonic current will create more core losses in the permanent magnets and rotor lamination. The excessive heat generated by the core losses can increase the magnet temperature and eventually cause an irreversible damage to the permanent magnets. Thirdly, the low frequency harmonic oscillation may cause stability issues of the electric machine drive system when it is interfacing with an AC grid. In addition, the control of the harmonics in power systems is particularly important to ensure the power quality [8].

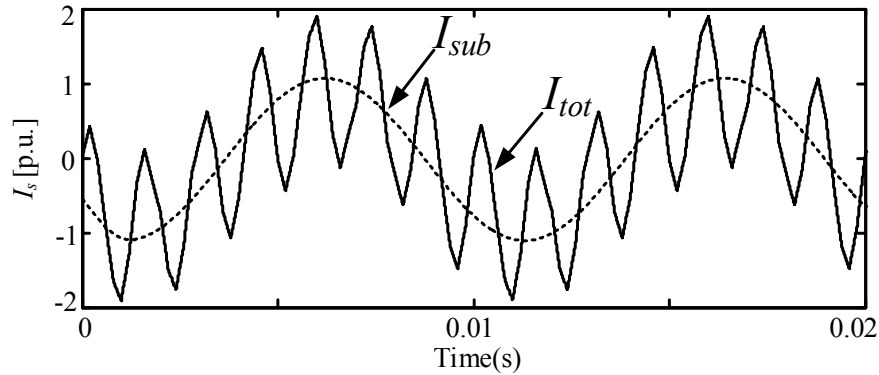


Figure 1.10: Phase current with obvious low frequency oscillation

In order to eliminate the low frequency harmonic components in the phase current, a control algorithm is developed to turn on and off the switches of the inverter exactly at the phase voltage command zero crossing points.

1.4 Literature Review

Many methods have been investigated to reduce the current THD for the PWM operation of inverters [5, 8–14]. Walker proposed a re-sampled uniform PWM technique to improve the performance of PWM for a multi-level converter [10]. Rahimi studied the subharmonic phenomenon in multi-converter vehicular power systems [13]. Chen compared the pulse width error of the digitized naturally sampled PWM and that of the naturally sampled PWM [11]. Stumpf verified that the sinusoidal PWM (SPWM), sinusoidal with third harmonic injection PWM (THI-PWM), and space vector modulation (SVM) techniques would generate lower frequency harmonic currents when the ratio m_f is low enough [9, 12]. Stumpf also

investigated the three different sampling techniques, regular sampled, naturally sampled, and oversampled in ultrahigh speed drive applications. He found out the subharmonic flux with considerable amplitudes can be generated, which cause high level of additional winding copper losses in rotor that could lead to damage of the machine [14]. Jordan investigated the patterns of subharmonics in flux linkage and current of a high speed induction machine drive system, as well as and the extra losses resulting from the subharmonics [15]. Halasz discussed that the subharmonic currents of inverter-fed ac drives would arise significantly if the ratio of the carrier-fundamental frequency was lower than 20-30 and investigated how naturally sampling and regular sampling affected the subharmonic current behavior for various discontinuous PWM methods [16, 17]. Bierhoff developed a new method of calculating the dc-link current harmonics for power converter operated by different PWM methods. The calculated dc-link current spectra at low carrier-fundamental frequency ratios is presented in the paper [18].

For the six-step control of three-phase inverters, a lot of efforts have been focused on how to achieve a smooth transition between the PWM and six-step operation to avoid any abrupt torque change, and the combination of six-step and current closed-loop control [7, 19–23]. Little work can be found on the low frequency oscillation problem of the six-step control caused by the digital sampling and control, particularly when the carrier-fundamental frequency ratio is decreasing. In fact, the digital control can cause similar issues for the PWM operation. However, the current closed-loop control is typically used in the PWM operation, which makes the low frequency harmonic current much less obvious compared with the

six-step operation that does not have a current closed-loop control function. These methods try to improve the current or dc voltage quality by using various types of sampling techniques for the PWM operation of power converters, or discuss the effects of the subharmonics and the harmonics phenomena in the converter systems. None discusses the low frequency issue and its reduction for the six step operation of a three-phase inverter.

1.5 Chapter Review

Chapter 2 introduces the causes of the low frequency harmonic components and the low frequency harmonic reduction algorithm. The reason for the existence of the low frequency harmonic components is that the switch can not be turned on or off at the voltage zero crossing points. In other words, the turn-on time and turn-off time are not identical. Digital implementation of PWM signal generation is also reviewed and its two different modes including the asymmetric mode and the symmetric mode are presented. The algorithm calculates the duty ratio when the phase voltage command crosses zero from positive to negative in one case and from negative to positive in the other case. After applying the control algorithm, the switch can be turned on and off exactly at the voltage zero crossing points.

Chapter 3 introduces the mathematical modeling and control algorithms of the PM synchronous machine. Reference frame transformation theory is presented. In addition, speed closed-loop SVPWM control and speed closed-loop direct voltage phase angle control are discussed.

Chapter 4 and 5 present simulation and experimental verifications by using both RL-load and interior permanent magnet synchronous machine load with and without the low frequency harmonic reduction algorithm. Both results show that the low frequency harmonic components in phase currents are reduced by more than 90%.

Chapter 6 summarizes the research work in this thesis and provides the potential future research work.

Chapter 2: Low Frequency Harmonic Production Mechanism and Principle of Low Frequency Harmonic Reduction Algorithm

This chapter presents the analog and digital implementation methods of PWM, and the reasons for the generation of the low frequency harmonic components of the phase currents in six-step operation. In addition, the principle of the low frequency harmonic reduction algorithm is also introduced. The algorithm calculates the duty ratio when the phase voltage command crosses zero. The switch can be turned on or off at the voltage zero crossing points after applying the reduction algorithm.

2.1 Principle of Analog PWM Signals Generation

In the case of analog circuits for PWM pulse generation or in simulations using tools such as Matlab, the PWM switching signals are generated by comparing a reference voltage signal and a high frequency carrier wave. The on- and off-status of the switch depend on whether the reference voltage signal is higher or lower than the carrier wave.

Typically, in real-world applications, a triangle wave generator and a comparator are used in the analog circuit to generate PWM signals. The triangle wave generator generates the carrier wave that is used to compare with the reference wave. The comparator takes the reference sine wave and the carrier as the inputs.

The output of the comparator is the PWM signal. As discussed in the chapter of Introduction, when the value of the triangle wave is greater than that of the input reference signal, the output of the comparator is low. On the other hand, when the value of the input reference signal is greater than that of the triangle wave, the output of the comparator is high.

SPWM, THI-PWM and SVPWM are widely used in AC electric machine drive controls. In SPWM, three reference sine waves V_a , V_b and V_c are compared with the carrier triangle wave. If the sine wave is larger than the carrier wave, the top switch of that phase leg of the inverter will be turned on. In THI-PWM control, a zero-sequence signal V_0 is computed from the three-phase sine waves. The modified sine waves are obtained by adding V_0 to the original three-phase sine waves. The output PWM signals are generated by comparing the modified sine waves with the triangle carrier wave. The SVPWM control is based on the voltage vector in the α, β or d, q plane [24]. It calculates the ON-time directly and it is often implemented in digital control.

2.2 Digital Implementation of PWM Algorithm

In the digital controller implementation, the ON time will be used to determine the duty ratio of the pulse or gate signals to the power switches in the inverter bridge, which will also result in the duty ratio of the switching signals [25]. Figure 2.1 demonstrates the definition of the duty ratio. The pulse width is the time that the signal is in the ON state and the period is the time of one switching cycle.

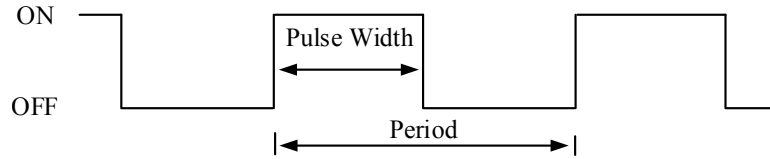


Figure 2.1: PWM signal waveform terms

The duty ratio D represents the percentages of the pulse width in one period. Therefore, it is defined as:

$$D = 100\% \times \frac{PulseWidth}{Period} \quad (2.1)$$

In a digital controller, the duty ratio will be calculated by reference wave V_{ref} and carrier wave $V_{carrier}$:

$$D = 100\% \times \frac{|V_{ref}|}{V_{carrier_{peak-to-peak}}} + 50\% \quad (2.2)$$

By using the calculated duty ratio and the switching cycle of the controller, the pulse width of the PWM signals can be computed. Therefore, the PWM signals are generated. In digital implementation, the counter inside the controller is applied to decide the turn-on time and turn-off time of the switches. Figure 2.2 shows the PWM signal and counter. It is important to notice that this is one of the counter types in digital implementation. At each switching cycle, the counter counts from 0 to N . Once the duty ratio is known, then the number of the counts N_D can be calculated to turn on or turn off the switches at the right time. The time cycle of each counts is the clock time of the controller and it usually is a constant number. Hence, the maximum counts N can be calculated based on the switching cycle.

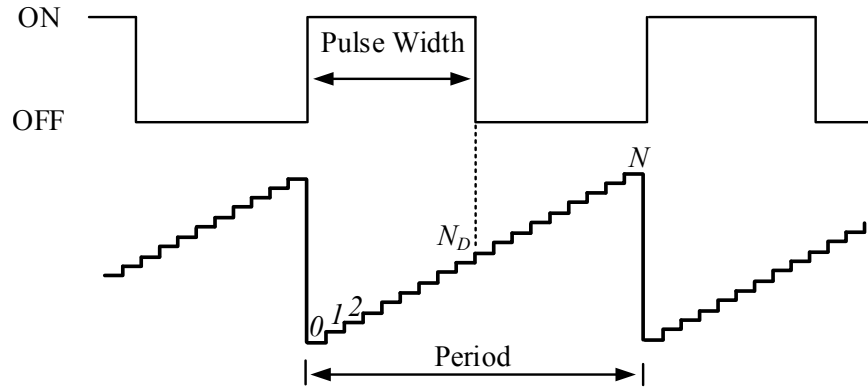


Figure 2.2: PWM signal waveform terms and counter wave

Symmetric and asymmetric modes can be used to create the PWM, as shown in Figure 2.3. T_c is the time that each count takes. For the symmetric PWM mode, the digital controller counts from 0 to N and back to 0, which is considered as one switching cycle, T_s . The duty cycle of a switch, D , is converted into a number of counts N_D . If the digital count matches N_D when it is counting up, the switch will be turned on. If the digital count matches N_D again when it is counting down, the switch will be turned off. It can be seen from Figure 2.3(a), the pulse is centered in one switching cycle.

For the asymmetric PWM mode, the digital controller counts from 0 to N in one switching cycle T_s . If the count matches N_D the switch will turn on, then turn off at the end of the switching cycle, as shown in Figure 2.3(c). If the PWM is configured to have the negative polarity, the switch will turn on at the beginning of one switching cycle and turn off when the count matches N_D , as shown in Figure 2.3(d). The pulse is located at either side of one switching cycle, instead of the center of the switching cycle.

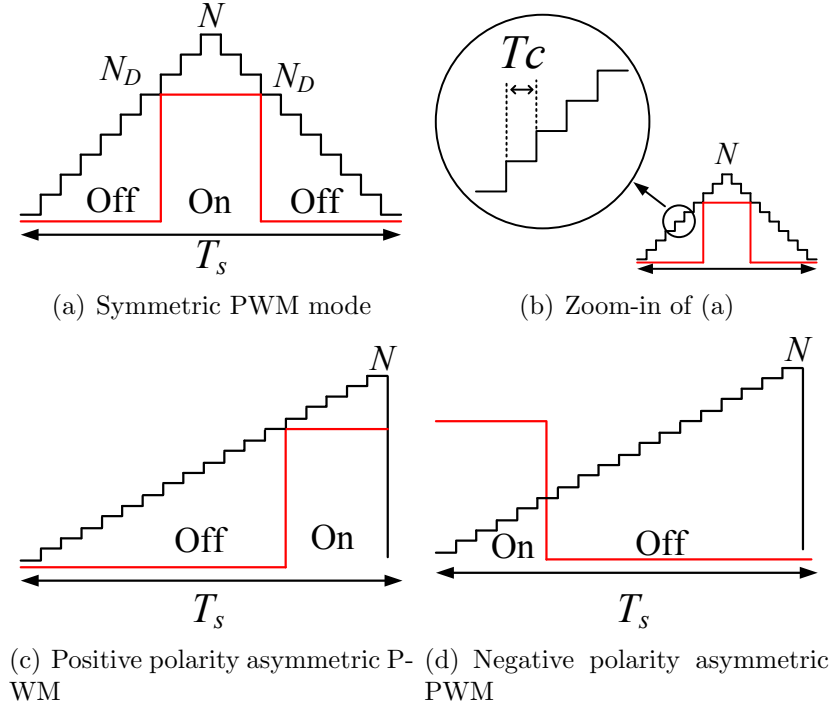


Figure 2.3: Digital implementation of PWM

In real applications, the PWM mode could be specified by changing the specific register in the PWM module of the controller. The switching frequency is related to the maximum digit counts N . In order to maintain the same switching cycle of the PWM signal, the maximum digit counts N in the asymmetric mode should be two times of that in the symmetric mode PWM.

In asymmetric PWM mode, the maximum number of counts can be calculated by:

$$N = \frac{T_s}{T_c} \quad (2.3)$$

where T_c is the clock time and T_s switching cycle.

In symmetric PWM mode, however, the counter counts from 0 to N during the first half switching cycle and counts back to 0 during the second half switching cycle. Therefore, the maximum number of counts are:

$$N = \frac{\frac{1}{2}T_s}{T_c} = \frac{1}{2} \frac{T_s}{T_c} \quad (2.4)$$

where T_c is the clock time and T_s switching cycle.

2.3 Principle of Low Frequency Harmonic Production

Before introducing the principle of the low frequency harmonic production, digital sampling methods are demonstrated. Figure 2.4 introduces three different types of digital sampling. Figure 2.4(a) demonstrates the symmetric sampling method. The counter counts from 0 to maximum number and back to 0 in one switching cycle. The samples are taken when it counts to 0 and the maximum number. Figure 2.4(b) introduces another type of symmetric sampling method. The samples are taken, however, when the counter only counts to 0. Figure 2.4(c) shows the asymmetric sampling method. The counter counts from 0 to the maximum number in one switching cycle and the samples are taken when the counter counts to 0.

SVPWM techniques are widely used due to increased utilization of V_{dc} , lower total harmonic distortion and switching loss. Three different SVPWM sampling techniques are introduced below [14].

The most commonly used method is regular sampled (RS)-SVPWM. It is convenient to implement by digital signal processor or by microcontroller. The input

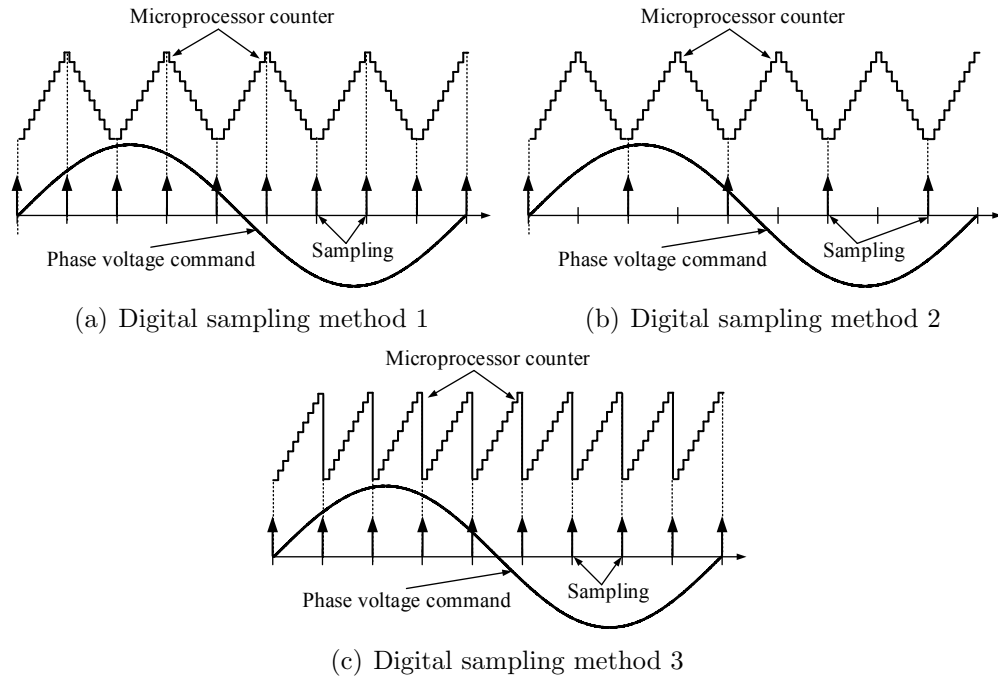


Figure 2.4: Digital sampling methods

signals are sampled at the beginning of every carrier period T_s . By decreasing the carrier-fundamental frequency ratio $m_f = f_s/f_1$, the accuracy of the RS-SVPWM is deteriorated as well. When m_f is low, due to the relative higher rotation speed of the reference voltage vector, the sampled voltage gets less accurate.

The second method is naturally sampled (NS)-SVPWM. In general, the NS-SVPWM in the past was implemented by using analog devices. up-to-date digital devices are used to implement the NS-SVPWM with higher accuracy. In addition, the NS-SVPWM is inclined to generate low frequency harmonic components with considerable amplitudes near given frequency ratios [14].

The third method is oversampled (O)-SVPWM. It increases the number of

samplings during one carrier period. Therefore, the accuracy of RS-SVPWM can be increased. The most common solution is to sample the input signals twice in each carrier period. The number of samples can be increased by using FPGA instead of microcontroller.

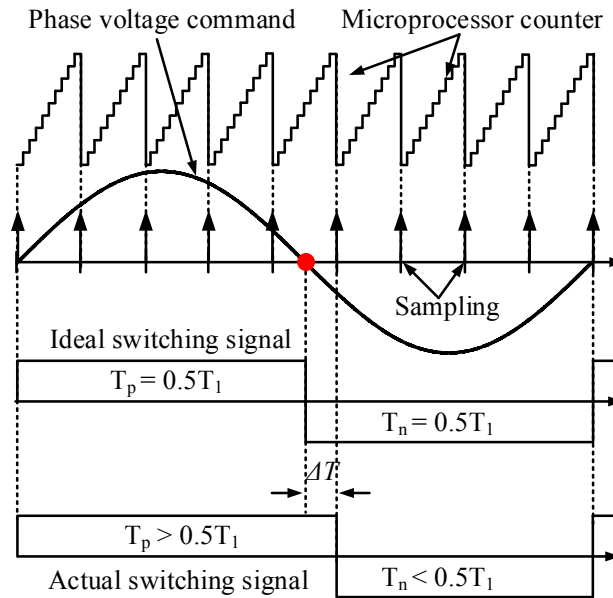


Figure 2.5: Principle of low frequency harmonic production

Figure 2.5 demonstrates how the low frequency oscillation current is produced in the six-step operation of a three-phase inverter due to the non-even integer carrier-fundamental frequency ratio, m_f . Here m_f is selected to be 9. The sampling and control are updated once every T_s . It is important to mention that the asymmetric sampling method is used to represent the counter.

The reference voltage of one phase and the counter are plotted. When the reference voltage is larger than zero, the top switch of this phase should be on. Otherwise the bottom switch is on. Ideally, the top switch of this phase should

turn off at the voltage zero crossing point. However, the voltage zero crossing point is in between two sampling points and the switching signal cannot be updated until the next sampling point (red solid circle point shown in the figure). Therefore, the actual turn-off of the top switch and turn-on of the bottom switch are delayed by ΔT . In this case, the top switch of this phase is turned on for more than half fundamental cycle. Meanwhile, the bottom switch of this phase is turned on for less than half fundamental cycle. This causes a DC offset in the phase voltage over one fundamental cycle that will result in a low frequency oscillation in the phase current. For a three-phase inverter, the phase shift between any two phases may not be 120° due to the non-even integer carrier-fundamental frequency ratio.

As long as the carrier-fundamental frequency ratio is not an even integer, the delay time of the turn-on and turn-off always occur and the switches can not be turned on or turned off at voltage zero crossing points. The value of the delay time is affected by the sampling frequency of the controller.

2.4 Principle of Low Frequency Harmonic Reduction Algorithm

The proposed low frequency harmonic reduction algorithm includes two different cases. The two cases are: 1) the reference voltage crosses zero from positive to negative and 2) the reference voltage crosses zero from negative to positive.

Figure 2.6(a) is used to demonstrate the principle of the control algorithm for the first case. In this case, the voltage zero crossing point is between α_1 and α_2 . The reference voltage at the current moment α_1 is known. The reference

voltage can be estimated for the next sampling point using the information of the fundamental frequency and the switching cycle. If the polarity of the voltage does not change for the next sampling point, the switch will remain on or off for this whole switching cycle. If the polarity of the voltage changes for the next sampling point, the duty ratio of the switches will be calculated and the PWM mode will be used for this switching cycle. Since the reference voltage is changing from positive to negative, an “on” signal will be generated at the beginning of the cycle and the switch will be turned off when α is equal to 180° . This requirement will be met by selecting the asymmetric PWM mode with negative polarity. The duty ratio can be expressed as:

$$D_{on} = \frac{|\alpha_1 - \pi|}{|\alpha_2 - \alpha_1|}, \alpha_2 = \alpha_1 + \omega_e \cdot T_s \quad (2.5)$$

where α_2 is the estimated voltage angle at the next sampling point, and ω_e the electrical angular velocity. The phase angle of the voltage can be calculated from the rotor angle position. It will be introduced in Chapter 4. In this case, the switch will be turned off exactly at the voltage zero crossing point.

Figure 2.6(b) shows the other case when the reference voltage goes from negative to positive. The zero crossing point of the voltage is at $\alpha = 0^\circ$. In this case, the pulse should be generated at the end of the switching cycle and the switch should be turned on when α is equal to 0° .

Therefore, the asymmetric PWM mode with the positive polarity will be cho-

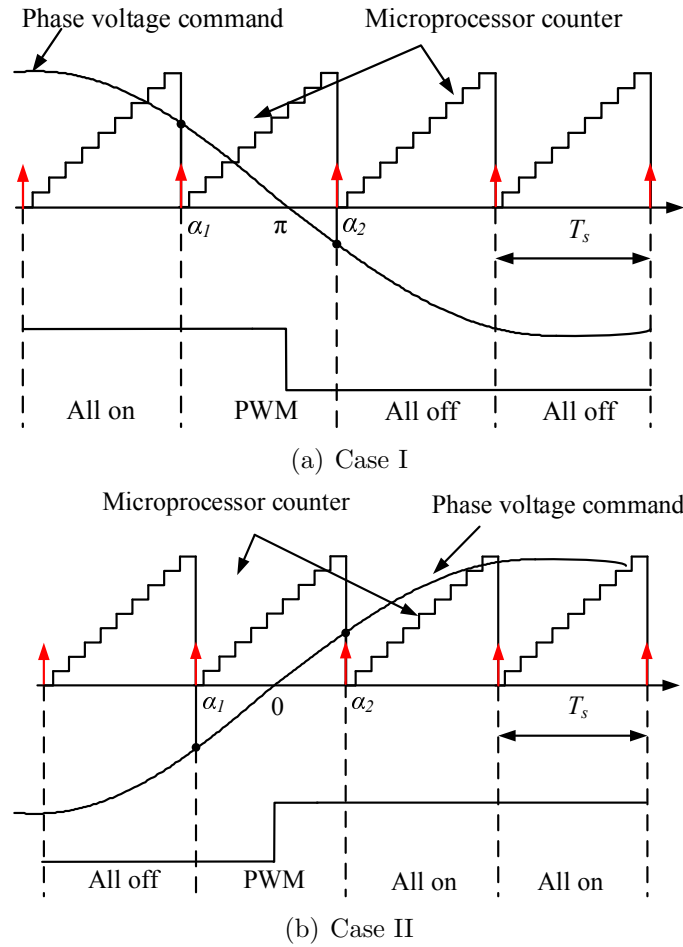


Figure 2.6: Low frequency harmonic reduction algorithm of Case I & II

sen. The duty ratio of the second case can be calculated as:

$$D_{on} = \frac{|\alpha_2 - 0|}{|\alpha_2 - \alpha_1|}, \alpha_2 = \alpha_1 + \omega_e \cdot T_s \quad (2.6)$$

2.5 Dead-time Effect and Short Pulse Elimination

The application of dead time is to avoid concurring turn-on of top and bottom power switches in one phase leg. Figure 2.7 shows the switching functions of top and bottom switches in one switching cycle and the dead time is T_{dead} .

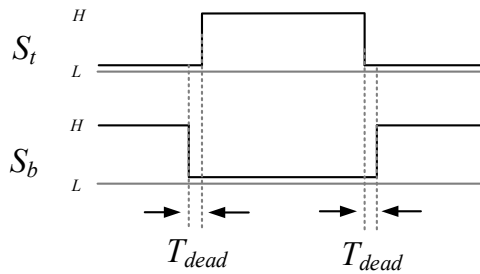


Figure 2.7: Dead time configuration

In six-step operation, the top switch should always be turned on when the reference voltage of that phase is positive and off when the reference voltage is negative. In hardware implementation, the duty ratio of the top switch is set to 1 when the reference voltage is positive. However, the dead time makes the actual duty ratio of the top switch $\frac{(T_s - T_{dead})}{T_s}$, which is less than one. As a result, the effect of the dead time will generate very short pulses that should be avoided in six-step operation. Figure 2.8 shows the switching signal of the top switch over one fundamental cycle with the dead time effect. Ideally, the switch should be on during the “All on” cycles, but the short pulses are created at the beginning and the end of each switching cycle due to the dead time of power switches. Simulations do not have this issue because the dead time can be zero without causing any DC bus shoot through issues.

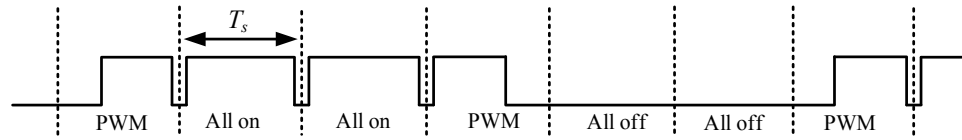


Figure 2.8: Switching signal with dead time configuration

In order to eliminate the short pulses, the dead time is set to zero if the polarity of the reference voltage does not change. Figure 2.9 shows the single phase configuration options for the dead-band submodule of the enhanced pulse width modulator module in the controller of TMS320F28333. The input of the dead-band submodule is the PWM signal of the top switch. During the normal operation, S_1 , S_2 and S_3 are configured as 1, 0 and 1 respectively. In this case, with the rising and falling edge delays, the top and bottom switching signals are same as those in the Figure 2.7. In six-step operation, whether the polarity of the reference voltage does or does not change, S_1 will be always set as 0 instead of 1. Since the switching signal of the bottom switch is inverted from the output of the falling-edge delay, no short pulse is caused by the delay. In this case, the PWM signal bypasses the rising-edge delay and then the short pulses are eliminated.

In order to understand the fundamental principle of the rising edge delay and falling edge delay modules, input and output waveforms of the modules are demonstrated in the Figure 2.10. The top wave is the original PWM signal, which is the input of both delay modules. The function of the rising edge delay is to postpone the rising time of the original signal. Meanwhile, the falling edge delay is used to postpone the falling time of the the original PWM signal.

In six-step operation, the delay time variables are set to 0 for both rising and

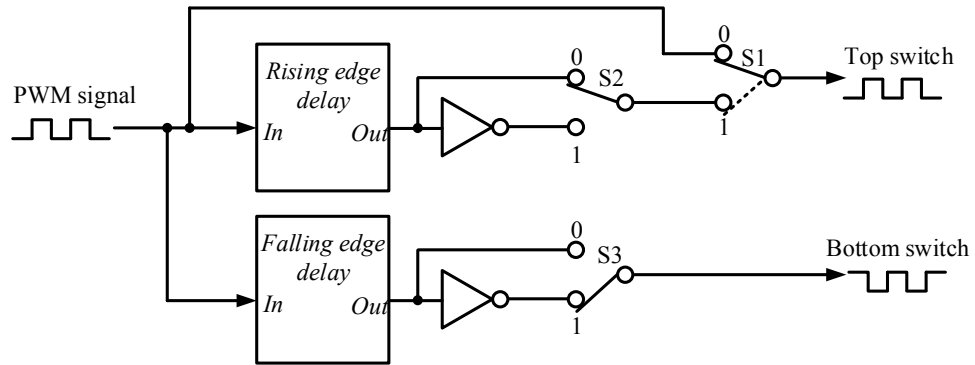


Figure 2.9: Configuration options for the dead-band submodule

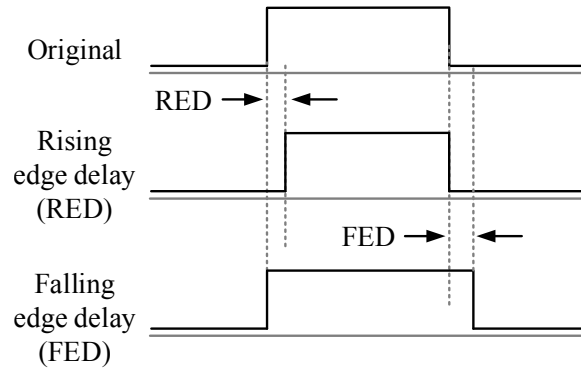


Figure 2.10: Dead-band waveforms

falling edge delay modules when the polarity of the reference voltage does not change. Therefore, the switching signals of the top and bottom switch do not have the dead time. When the reference voltage changes from positive to negative or negative to positive, the delay time variables of the two modules are not equal to 0. The top switch still does not have the dead time since S_1 is set to 0. The falling edge delay module enables the delay time of the bottom switch to avoid short circuit of the phase leg.

Figure 2.11 compares the switching signals with and without the short pulse

elimination from the experiment results. The top waveform is the switching signal with all short pulses eliminated and the bottom waveform is the switching signal with short pulses caused by the dead-time effect.

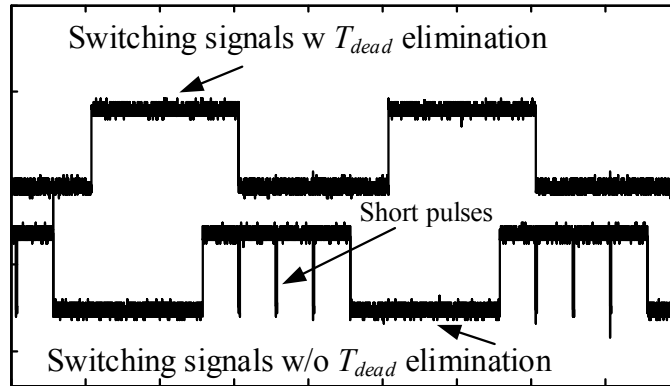


Figure 2.11: Short pulses elimination

Chapter 3: Mathematical Modeling and Control Algorithms of PM Synchronous Machines

This chapter presents the reference frame transformation theory, mathematical modeling of PM synchronous machines, and the control algorithms of the PM synchronous machine that is used in the simulations and hardware experiment.

3.1 Reference Frame Transformation Theory

Since the inductances of the AC electric machine vary with the real rotor position, the voltage equations are time-varying differential equations when the electric machines are rotating. Using the reference frame transformation theory in the steady-state, the variables of an AC machine can simplify the analysis by converting the time-varying differential equations to the time-invariant differential equations.

Figure 3.1 shows the combined representation of the three phase components in the three-phase (f_a , f_b and f_c) reference frame (solid), orthogonal stationary (f_α and f_β) reference frame (dash) and orthogonal rotating (f_d and f_q) reference frame (dot) or called d - q reference frame. The three-phase reference frame and orthogonal stationary reference frame are both stationary. The d - q reference frame is rotating with the rotor of the AC machine. In the three-phase stationary reference frame, each axis has 120° apart; while in both the orthogonal stationary and rotating

reference frame, each axis has 90° apart.

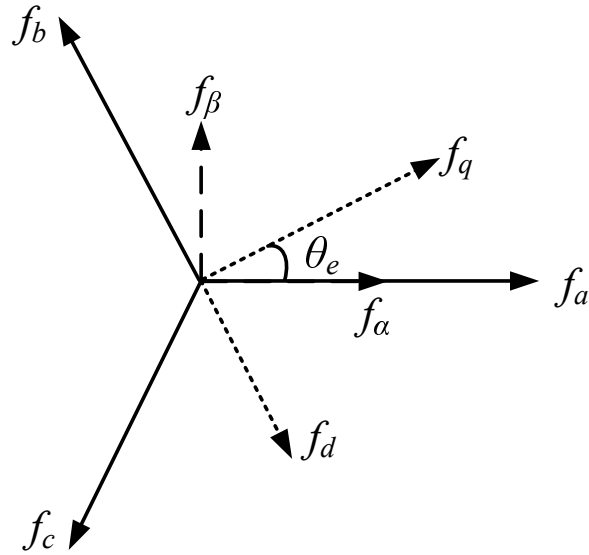


Figure 3.1: Combined several reference frames

In the steady-state, the electrical variables including the three-phase voltage, current and magnetic flux in the three-phase stationary reference frame can be transformed into two constant variables in the d - q reference frame by two steps. The first step is that the three-phase variables are transformed to two variables in the orthogonal stationary reference frame. The α -axis here is same as the a -axis of the three-phase reference frame, and the β -axis leads α -axis by 90° . At the second step, by knowing the rotor speed and angle, the two variables in the orthogonal stationary reference frame can be transformed into two constant variables in d - q axis, which rotates at the same speed as the rotor. The d -axis represents the direction of the main flux of the permanent magnet, and the q -axis leading d -axis by 90° .

According to the complex vector theory [26], the three phase quantities can be represented by the following vectors in the three-phase stationary reference frame:

$$\vec{f}_a = f_a(t) \cdot e^{j0} \quad (3.1)$$

$$\vec{f}_b = f_b(t) \cdot e^{j\frac{2\pi}{3}} \quad (3.2)$$

$$\vec{f}_c = f_c(t) \cdot e^{-j\frac{2\pi}{3}} \quad (3.3)$$

where e^θ is a unit vector with an angle θ .

The total space vector, which is a single vector rotating in the stationary reference frame, can be represented by the three phase components:

$$\vec{f}_s = \frac{2}{3}(\vec{f}_a + \vec{f}_b + \vec{f}_c) \quad (3.4)$$

Among the various transformation methods, the clarke transformation and park transformation are widely used in the vector control architecture related to AC machines. The clarke transformation converts the three-phase quantities into two-phase quadrature quantities in an orthogonal stationary reference frame, which is considered as the first step mentioned in the previous paragraph. At the second step, the park transformation converts the two-phase stationary system into a two-phase rotating reference frame that is the d - q reference frame. The angle θ_e is the rotation angle between the q -axis and α -axis.

In order to transform the three-phase time-varying variables into time-invariant variables, the first step is to apply the clarke transformation. The following trans-

formation matrix represents the clarke transformation:

$$\begin{bmatrix} f_\alpha \\ f_\beta \\ f_0 \end{bmatrix} = \frac{2}{3} \begin{bmatrix} 1 & -\frac{1}{2} & -\frac{1}{2} \\ 0 & \frac{\sqrt{3}}{2} & -\frac{\sqrt{3}}{2} \\ \frac{1}{2} & \frac{1}{2} & \frac{1}{2} \end{bmatrix} \begin{bmatrix} f_a \\ f_b \\ f_c \end{bmatrix} \quad (3.5)$$

where the zero sequence component is used to enable the invertibility of the clarke transformation matrix.

Its inverse transformation represented as:

$$\begin{bmatrix} f_a \\ f_b \\ f_c \end{bmatrix} = \begin{bmatrix} 1 & 0 & 1 \\ -\frac{1}{2} & \frac{\sqrt{3}}{2} & 1 \\ -\frac{1}{2} & -\frac{\sqrt{3}}{2} & 1 \end{bmatrix} \begin{bmatrix} f_\alpha \\ f_\beta \\ f_0 \end{bmatrix} \quad (3.6)$$

Although the three-phase variables are converted to two-phase variables, the two phase components f_α and f_β in the orthogonal stationary reference frame are still varying with time. Hence, the three-phase voltage, current, flux linkage and inductance in an AC rotating machine are still rotor position dependent and time varying.

In order to convert the two phase quantities from time-varying to time-invariant, the park transformation is introduced and expressed by the following matrix:

$$\begin{bmatrix} f_d \\ f_q \end{bmatrix} = \begin{bmatrix} \sin \theta_e & -\cos \theta_e \\ \cos \theta_e & \sin \theta_e \end{bmatrix} \begin{bmatrix} f_\alpha \\ f_\beta \end{bmatrix} \quad (3.7)$$

where θ_e is the electrical angle between the q -axis and α -axis. f_d and f_q are two rotating vectors rotate as the same speed as the orthogonal rotating reference frame. Therefore, vectors on the d - and q -axis appear as constant values.

Similarly, the two-phase rotating reference frame can be transformed to the stationary reference frame by applying the inverse park transformation, which is expressed below:

$$\begin{bmatrix} f_\alpha \\ f_\beta \end{bmatrix} = \begin{bmatrix} \sin \theta_e & \cos \theta_e \\ -\cos \theta_e & \sin \theta_e \end{bmatrix} \begin{bmatrix} f_d \\ f_q \end{bmatrix} \quad (3.8)$$

The transformation methods that convert time-varying variables to time-invariant variables are not unique. These transformations are based on the conservation of energy. Most of the AC three-phase electric machines such as PM machines, induction machines and doubly-fed induction machines apply the clarke and park transformations that are discussed above.

3.2 Mathematical Modeling in Rotating Reference Frame and Torque Equations of PM Machines

In the steady-state, based on the reference frames theory, the voltage equations of a PM synchronous machine in the orthogonal rotating reference frame can be expressed as:

$$\begin{bmatrix} v_d \\ v_q \end{bmatrix} = \begin{bmatrix} R_s & -\omega_e L_q \\ \omega_e L_d & R_s \end{bmatrix} \begin{bmatrix} i_d \\ i_q \end{bmatrix} + \lambda_m \omega_e \begin{bmatrix} 0 \\ 1 \end{bmatrix} + \begin{bmatrix} L_d \frac{di_d}{dt} \\ L_q \frac{di_q}{dt} \end{bmatrix} \quad (3.9)$$

where v_d and v_q are d - and q -axis components of the stator terminal voltage; i_d and i_q are d - and q -axis components of the stator terminal current; R_s is the resistance of phase winding; L_d and L_q are d - and q -axis components of the armature winding self-inductance; λ_m is the flux linkage of the permanent magnet and ω_e is the electrical rotor angular velocity.

Neglecting the inductive and resistive voltage drop terms, the voltage equations of a PM machine in the orthogonal rotating reference frame at the steady state can be written as:

$$\begin{bmatrix} v_d \\ v_q \end{bmatrix} = \begin{bmatrix} 0 & -\omega_e L_q \\ \omega_e L_d & 0 \end{bmatrix} \begin{bmatrix} i_d \\ i_q \end{bmatrix} + \lambda_m \omega_e \begin{bmatrix} 0 \\ 1 \end{bmatrix} \quad (3.10)$$

By using the d - and q -axis voltage components to represent the currents, the steady state d - q currents can be approximated as:

$$\begin{aligned} i_d &= \frac{v_q}{\omega_e L_d} - \frac{\lambda_m}{L_d} \\ i_q &= -\frac{v_d}{\omega_e L_q} \end{aligned} \quad (3.11)$$

According to the equation of the output torque of a PM synchronous machine, which is shown below, the relationship between the output torque and the machine speed is proportional under the constant load situation.

$$T_e = T_l + B\omega_m + J\frac{d\omega_m}{dt} \quad (3.12)$$

where T_e is the output electromagnetic torque, T_l the torque of the load, B the coefficient of the friction, ω_m the mechanical angular velocity of the rotor and J the moment of inertia.

The output torque can be controlled by the stator current of the machine. The torque can be also calculated from the current. The equation is expressed as:

$$T_e = \frac{3P}{2} [\lambda_m i_q + (L_d - L_q) i_d i_q] \quad (3.13)$$

where P is the number of poles of the electric machine, λ_m the flux linkage of the permanent magnet, L_d the d -axis inductance and L_q the q -axis inductance.

As introduced in the previous section, the three-phase current in the stator windings can be converted to a rotating vector that can also be decomposed into the d - and q -axis. The flux linkage of the permanent magnet λ_m and the d - q inductance can be assumed as constant, the output torque can be controlled by the current.

3.3 PWM Control

Figure 3.2 shows the block diagram of a PM synchronous machine using the SVPWM with speed closed-loop control.

The commonly used controllers for the speed and current control can be proportional integral (PI) controllers. For the stator current vector, the d -axis is aligned with the axis of the north pole of the permanent magnets of the electric machines

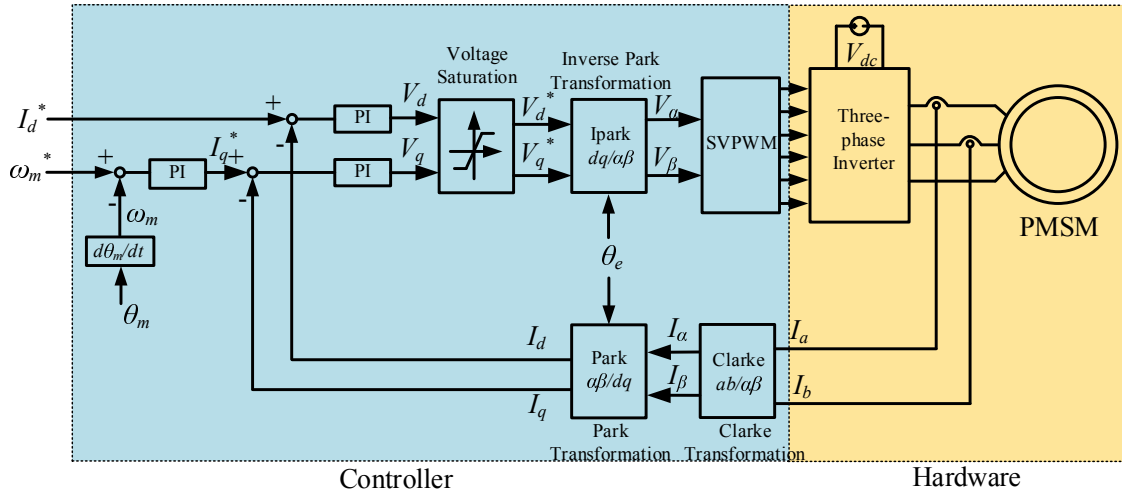


Figure 3.2: Block diagram speed closed-loop SVPWM control of PM synchronous machine

and the q -axis leads the d -axis by 90 degrees. The flux linkage of the rotor can be controlled by the d -axis component of the current vector and the output torque is controlled by the q -axis component of the current vector.

Due to the positive correlation between the q -axis current and output torque if the d -axis current is given by a constant, a PI speed regulator is applied. The speed PI regulator generates the q -axis reference current. For the current closed-loop, the d -axis current and q -axis current regulator produce the d -axis and q -axis voltage commands respectively.

Inverse park transformation is applied to convert the reference voltage V_d and V_q to V_α and V_β in the stationary frame. Two variables V_α and V_β are taken as the inputs of the space vector control algorithm block. The rotor angle position θ_m is converted to the electrical angle θ_e , that is used for the park and inverse park transformations.

3.4 Six-step Control

Figure 3.3 shows the control diagram of a PM machine using six-step with the speed closed-loop voltage phase angle control.

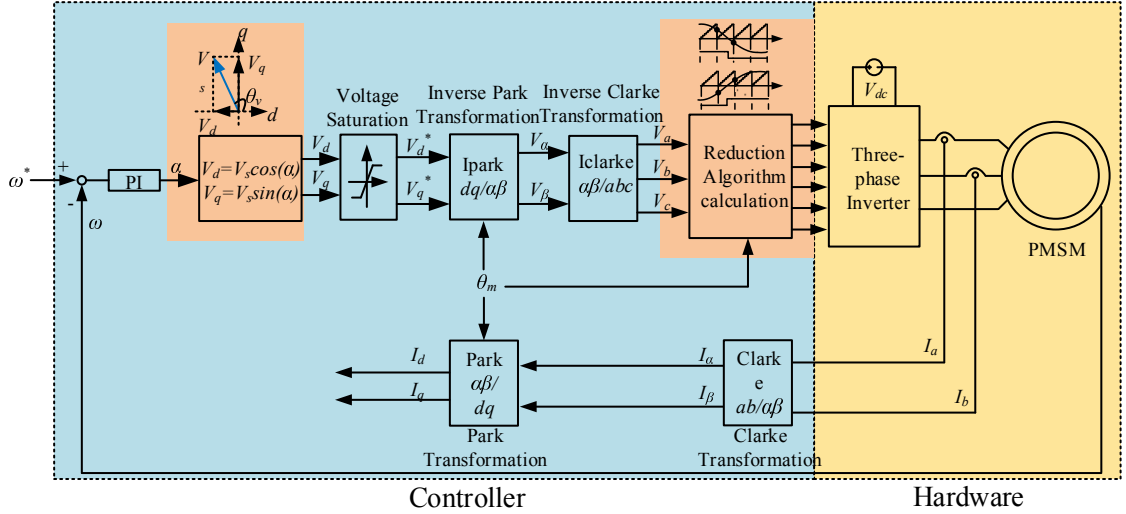


Figure 3.3: Block diagram speed closed-loop voltage phase angle control in six-step operation of PM synchronous machine

Based on the output torque equation Eq. (3.13), the output torque can be expressed by substituting Eq. (3.11) into Eq. (3.13):

$$T_e = -\frac{3P}{4\omega_e^2 L_d L_q} [v_d \lambda_m \omega_e L_q + (L_d - L_q) v_d v_q] \quad (3.14)$$

In six-step operation, the magnitude of the fundamental components of the phase voltage is $\frac{2}{\pi} V_{dc}$ [6]. Figure 3.4 shows the fundamental component of the input terminal voltage on the d - q plane in six-step operation of a PM synchronous machine. The phase angle θ_v is defined as the angle between voltage v_s and the

positive d -axis. Therefore, the phase voltage v_s can be decomposed into v_d and v_q as:

$$\begin{aligned} v_d &= v_s \cos \theta_v \\ v_q &= v_s \sin \theta_v \end{aligned} \quad (3.15)$$

The torque equation Eq. (3.14) can be rewritten by substituting Eq. (3.15) into Eq. (3.14):

$$T_e = -\frac{3P}{8\omega_e^2 L_d L_q} [2\lambda_m \omega_e L_q v_s \cos \theta_v + (L_d - L_q) v_s \sin 2\theta_v] \quad (3.16)$$

In six-step operation, since the dc bus voltage is fixed, the fundamental component of the input terminal voltage v_s is also a constant variable. Hence, the output torque can be only controlled by adjusting the voltage phase angle θ_v at a constant speed.

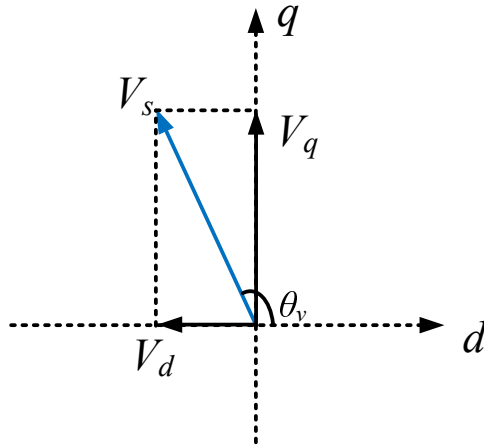


Figure 3.4: Definition of V_s and θ_v

Voltage phase angle control algorithms by adjusting the phase angle θ_v are proposed in [7, 27–30] as well. The phase angle could be directly calculated from the Eq. (3.16) by given the reference torque T_e and rotating speed ω_e of the machine, or it can be adjusted by a PI regulator to take the reference speed and feedback speed of the machine as the inputs. The PI regulators of the currents will be removed since the magnitude of the phase voltage is fixed and the current can not be controlled.

The voltage phase angle PI regulator takes the error of the command speed and actual speed as the input, and then produces a voltage reference angle θ_v that contains the torque information. The d - and q - axis reference voltages could be calculated by using Eq. (3.15). V_s is the maximum available phase voltage magnitude. Inverse park and inverse clarke transformation will be taken to convert the voltage into a three-phase voltage command. As discussed in Chapter 2, the reduction algorithm takes fundamental frequency, switching cycle and the voltage angle to calculate the duty ratio when the polarity of the phase voltage changes. In addition, the voltage angle of each phase could be converted from the rotor angle position. In this thesis, the rotor angle position is defined as the angle between the q -axis and phase A axis as shown in the figure 3.5. Therefore, the phase angles of the three-phase voltage V_a , V_b and V_c can be represented as:

$$\theta_a = \theta_v + \theta_e \quad (3.17)$$

$$\theta_b = \theta_v + \theta_e - \frac{2\pi}{3} \quad (3.18)$$

$$\theta_c = \theta_v + \theta_e + \frac{2\pi}{3} \quad (3.19)$$

where θ_v is the voltage phase angle and θ_e the rotor angle position.

Once the phase angles of each phase are known, duty ratios of the switches in each phase leg of the inverter can be calculated. The voltage zero crossing points can also be detected by using the phase voltage magnitude from the inverse clarke transformation. For the direct voltage phase angle control discussed above, the feedback currents I_d and I_q are only used for monitoring.

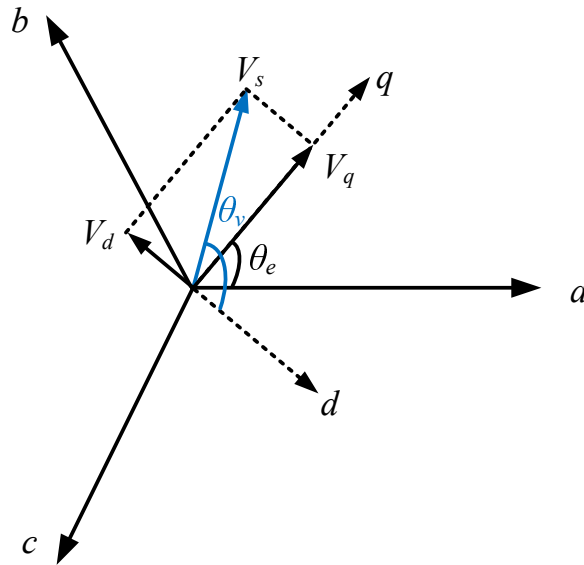


Figure 3.5: Voltage vector in $d-q$ and abc reference frame

Chapter 4: Simulation Verification

Simulations were performed to verify the the proposed low frequency harmonic current reduction control algorithm for the six-step operation of a three-phase inverter. Both a three-phase RL load and an interior permanent magnet synchronous machine were simulated respectively. This chapter presents the simulation results.

4.1 Simulation Results of RL load

The simulation software Powersim (PSIM) was used to simulate the low frequency current oscillation phenomenon and verify the proposed control algorithm using the RL load. PSIM can simulate control circuit in various forms: in analog circuit, s-domain transfer function block diagram, z-domain transfer function block diagram and custom C code. The custom C code provides the opportunity for users to implement the digital control in the simulation.

Figure 4.1 shows the schematic of the simulation model including a microcontroller, a three-phase power inverter, and a three-phase RL load. The control is implemented in the digital form using C language to simulate the real-world digital control.

The dc bus voltage was set to be 30 V. The load resistance and inductance are 2 Ohms and 0.8 mH. The fundamental frequency f_1 was 1.1 kHz and the switching

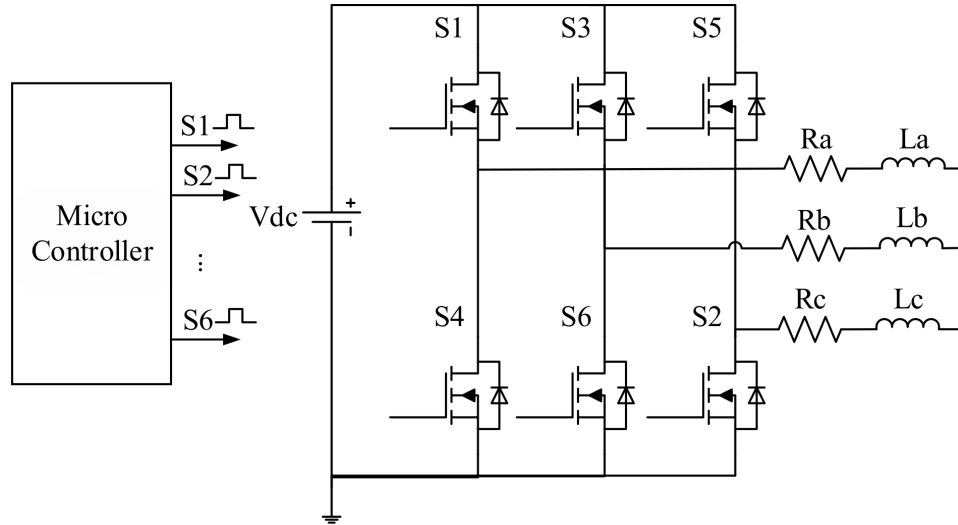
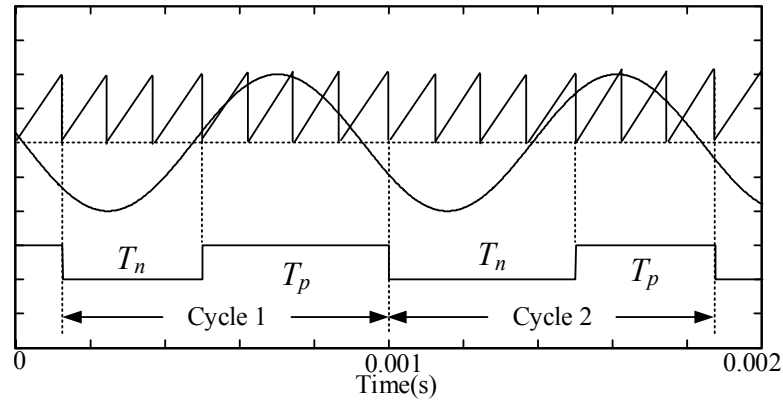


Figure 4.1: Schematic of simulation system using RL load

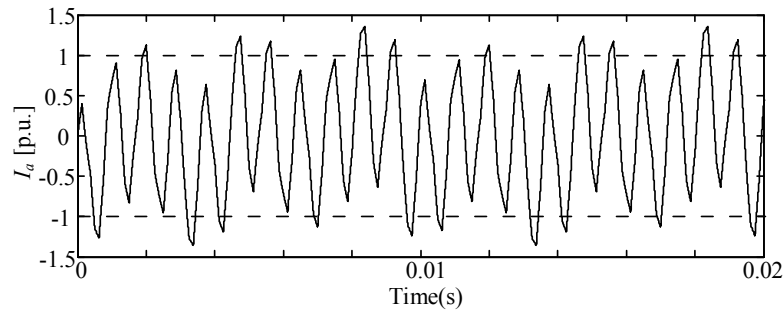
frequency f_s was 8 kHz.

Figure 4.2(a) shows the simulation results of the phase A switching signal without applying the low frequency harmonic reduction algorithm. It can be seen that the top switch is turned on for a longer time than the bottom switch in cycle 1. In cycle 2, the top switch is turned on for a shorter time than the bottom switch. Due to the asymmetric pulse width of the switching signal, the low frequency components are generated in the phase current as shown in Figure 4.2(b). Here 1 p.u. current is defined as the maximum value of the phase current when the circuit is operated at six-step mode.

Figure 4.3(a) shows the simulation results of the phase A switching signal after applying the low frequency harmonic reduction algorithm. The turn-on time and turn-off time of the top switch are equal to each other. The top and bottom switches of the power inverter are turned on and off exactly at the zero crossing points of



(a) Reference voltage, carrier wave, and switching signals of Phase A

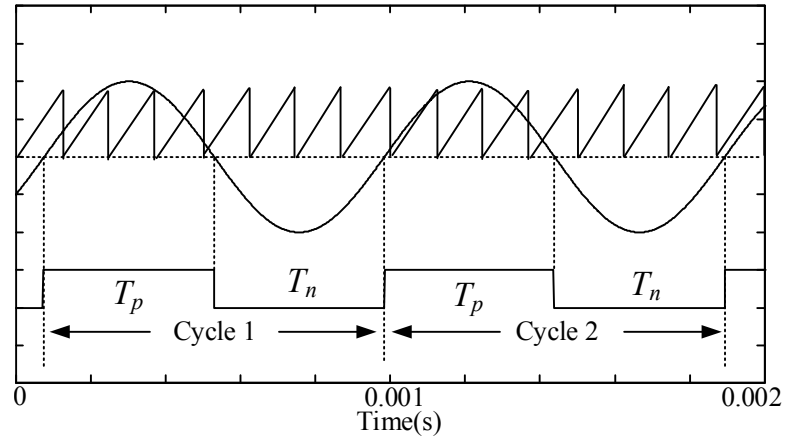


(b) Phase A current with low frequency harmonic component

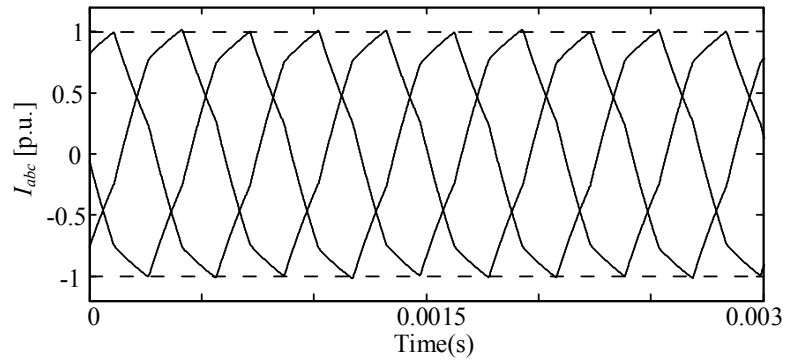
Figure 4.2: Simulation results: switching signals and current of Phase A without using low frequency harmonic reduction algorithm

the command phase voltage. Figure 4.3(b) demonstrates the three-phase current after applying the low frequency harmonic reduction algorithm. The low frequency harmonic components are significantly reduced and the phase shift between any two phases is 120° .

The spectrum analyses of the phase A current before and after applying the proposed control algorithm are illustrated in Figure 4.4. The magnitude of the current is displayed using the logarithmic scale to clearly show the values of low



(a) Reference voltage, carrier wave, and switching signal of Phase A



(b) Three-phase current without low frequency harmonic component

Figure 4.3: Simulation results: switching signal and three-phase current applying low frequency harmonic reduction algorithm

frequency harmonic components. Before the low frequency harmonic reduction algorithm is applied, the two dominant low frequency components are 300 Hz and 100 Hz. The magnitudes of the 300-Hz and 100-Hz components reduce from 0.35 p.u. and 0.13 p.u. down to 0.016 p.u and 0.003 p.u.

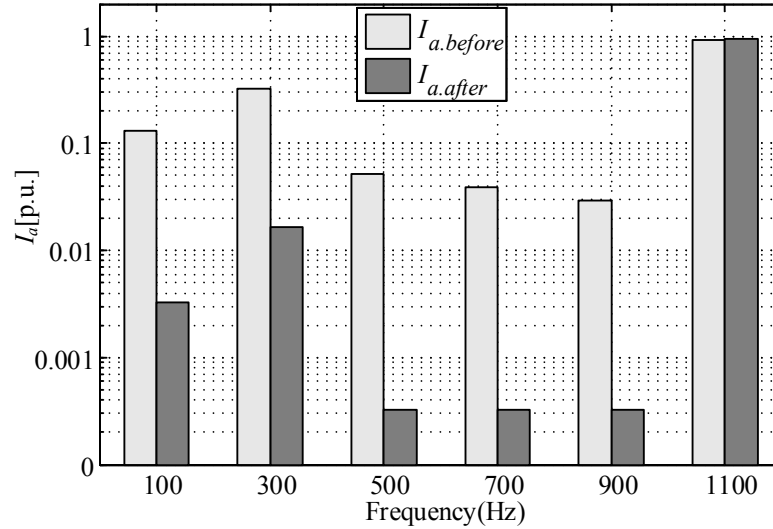


Figure 4.4: Simulation results: spectrum analysis of Phase A current before and after applying low frequency harmonic reduction algorithm

4.2 Simulation Results of Interior Permanent Magnet Synchronous Machine Load

Simulation results of a three-phase RL load clearly show that the low frequency harmonic components are reduced significantly after applying the reduction algorithm. An interior permanent magnet synchronous machine was also simulated to verify the low frequency harmonic reduction algorithm.

The simulation was performed in MATLAB/Simulink software. Figure 4.5 shows the schematic of the simulation control diagram. The open-loop control is implemented in the simulation and the inputs of the control system are d -axis and q -axis command voltages. A triggered subsystem using a counter function was applied in the simulation to perform as a digital controller. The machine is running

at a constant speed of ω_r under speed mode in simulation. Therefore, changing the variables of V_d and V_q affect the torque and phase currents of the electric machine.

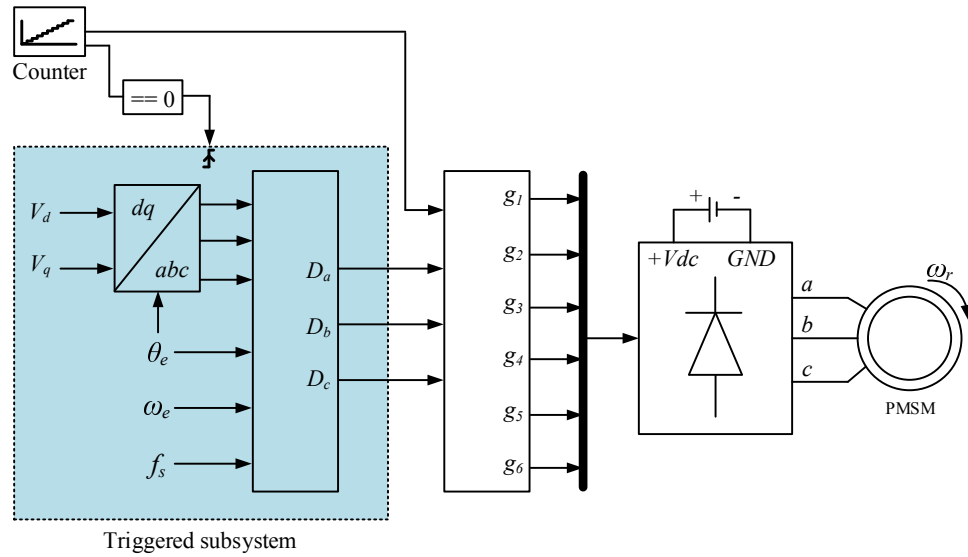


Figure 4.5: Schematic of simulation system using machine load

In simulation, the machine and power electronics model is running at $0.2 \mu s$ rate and the control is updated once every $250 \mu s$ which is synchronized with the switching frequency. Some key machine parameters are listed in Table 4.1.

Table 4.1: Ratings and parameters of the PM machine

Rated current	500 A
d-axis inductance	0.15 mH
q-axis inductance	0.25 mH
Flux linkage of PM	0.0557 V·s
Number of poles	8
Switching frequency	4 kHz
Stator dc resistance	0.01 Ω

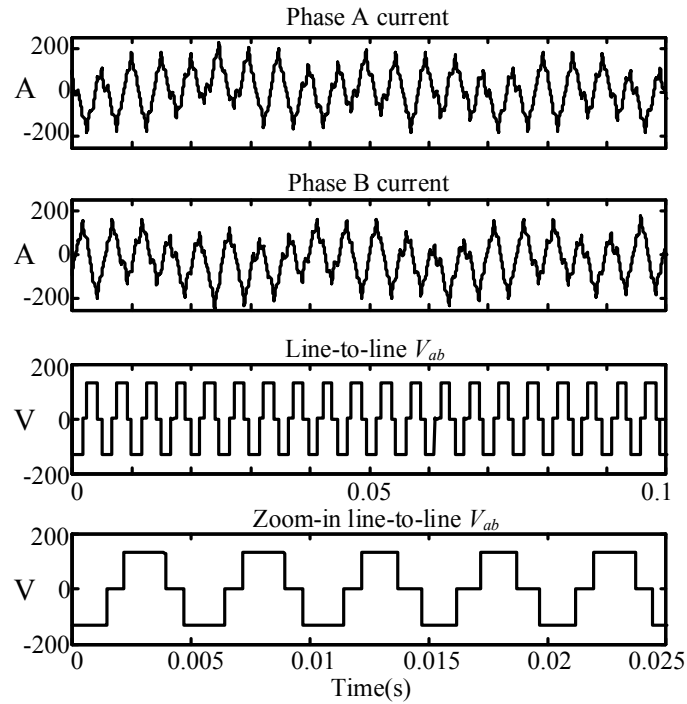
The dc bus voltage V_{dc} was set to be 130 V in the simulation. The IPM machine speed command was 3030 rpm corresponding to 202 Hz in terms of the electrical frequency. The carrier-fundamental frequency ratio m_f was 19.8, which is not an integer. The non-integer carrier-fundamental frequency ratio generated the low frequency harmonic components in the phase currents.

Figure 4.6(a) demonstrates the phase currents I_a and I_b , and a line-to-line voltage V_{ab} before applying the low frequency harmonic reduction algorithm. The low frequency harmonic components are obvious in the phase currents. The zoom-in of the line-to-line voltage also shows that the top and bottom switches of one phase leg are not turned on for the same amount of time over one fundamental cycle. Figure 4.6(b) shows the phase currents and the line-to-line voltage after implementing the low frequency harmonic reduction algorithm. The low frequency harmonic components in phase currents are significantly reduced.

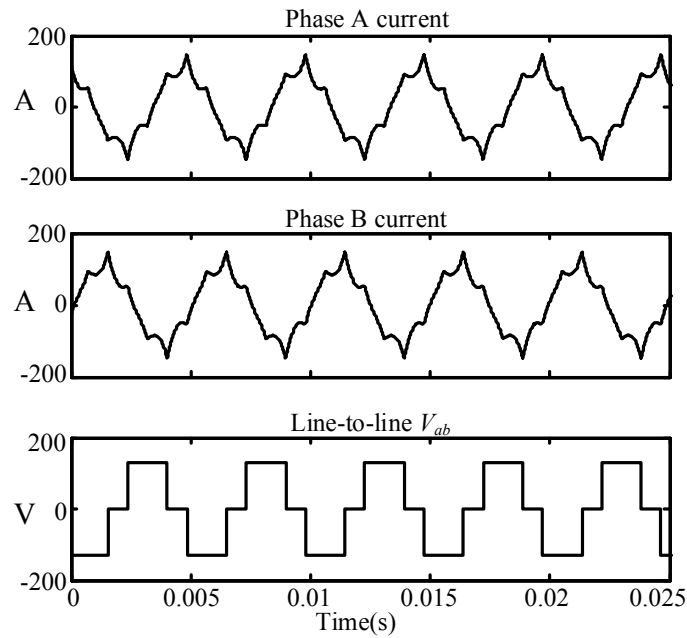
Spectrum analyses of the phase A current before and after applying the low frequency harmonic reduction algorithm were conducted by using the Spectrogram function in Matlab. Figure 4.7 presents the spectrogram of the phase A current for a period of 3 seconds. The objective of the function is to describe how the spectral content of a signal is changing in time [31]. The x -axis represents the frequency of the current covering up to 3000 Hz. The color bar represents the distribution of the power density of various harmonics of the phase current in dB/Hz.

The spectrogram of the phase current before applying the reduction algorithm shows abundant low frequency harmonics. In addition, the frequencies and magnitudes of the low frequency harmonics are varying with time. After applying the

reduction algorithm, the spectrogram shows that the fundamental component (202 Hz) is dominant and the low frequency harmonic components are significantly reduced. Both spectrograms clearly show the 5th, 7th, 11th, and 13th harmonics in the phase current, which is a signature of the six-step control.



(a) Simulation results: Phase currents I_a & I_b , line-to-line voltage V_{ab} , and zoom-in line-to-line voltage V_{ab} before applying the low frequency oscillation reduction algorithm



(b) Simulation results: Phase currents I_a & I_b , and line-to-line voltage V_{ab} after applying the low frequency oscillation reduction algorithm

Figure 4.6: Simulation results: Phase currents I_a & I_b , and line-to-line voltage V_{ab} before and after applying the low frequency harmonic reduction algorithm

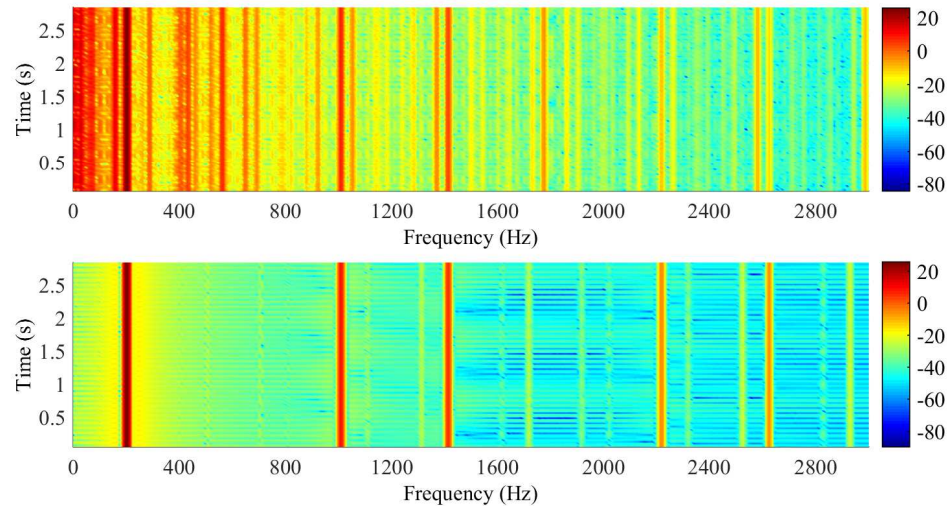


Figure 4.7: Spectrum analysis of Phase A current before and after applying low frequency harmonic reduction algorithm

Chapter 5: Experimental Verification

In addition to simulation verification, experimental test results using the three-phase RL load and the interior permanent magnet synchronous machine with and without the proposed reduction algorithm are presented in this chapter.

5.1 Experimental Results using RL load

Experimental testing was conducted to verify the proposed low frequency harmonic reduction algorithm using a three-phase RL load. Two different carrier-fundamental frequency ratios were selected in the testing. The first test case used the same fundamental and switching frequencies as in the simulations in the previous section. In addition, in order to verify the low frequency harmonic reduction algorithm with lower frequency ratio, 1700 Hz was selected as the fundamental frequency and the switching frequency still remained 8 kHz, the same as the sampling frequency. In this case, the carrier-fundamental frequency ratio m_f was equal to 4.7.

Figure 5.1 is a picture of the hardware testing system. The DC input voltage of the three-phase inverter was 30 V. The resistance and inductance of each phase are 2 Ohms and 0.8 mH. A dSPACE controller, DS1104, was used as the digital controller. The control algorithm was hand coded using C language to enable the

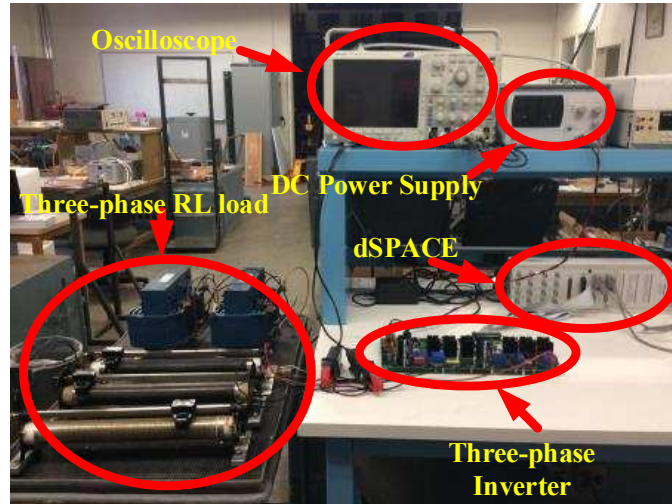


Figure 5.1: Hardware testing system using RL load

asymmetric PWM function.

Figure 5.2 shows the switching signals of the top three switches when the fundamental frequency f_1 is 1100 Hz without applying the low frequency harmonic reduction algorithm. The switching status of each switch can only be updated at the sampling points. The testing results are consistent with the PSIM simulation results. For each phase, the turn-on time of the top switch is either longer ($T_p \geq 0.5T_s$) or shorter ($T_p \leq 0.5T_s$) than that of the bottom switch. In addition, the phase shifts between the switching signals of every two phases are not equal to 120° . For instance, the phase shift between switching signals of two phases θ_{AB1} is 115 degrees. At another moment, this phase shift θ_{AB2} becomes 92 degrees.

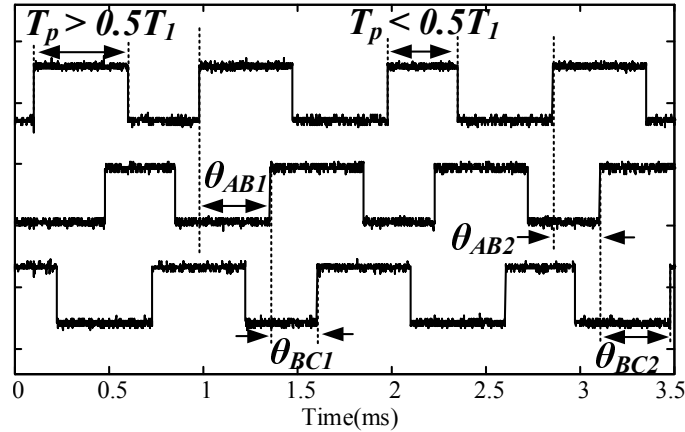
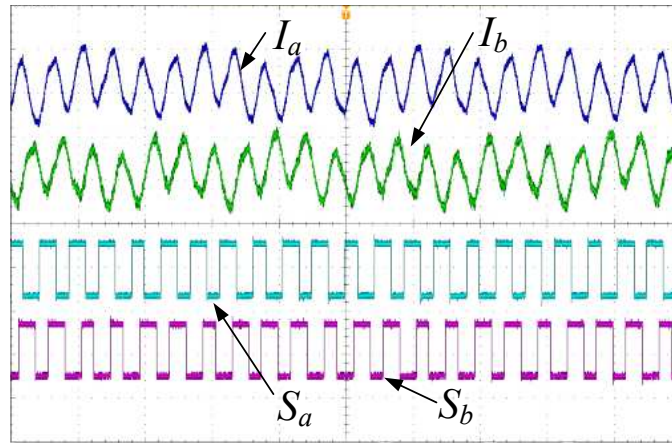


Figure 5.2: Experimental results: three-phase switching signals without applying low frequency harmonic reduction algorithm

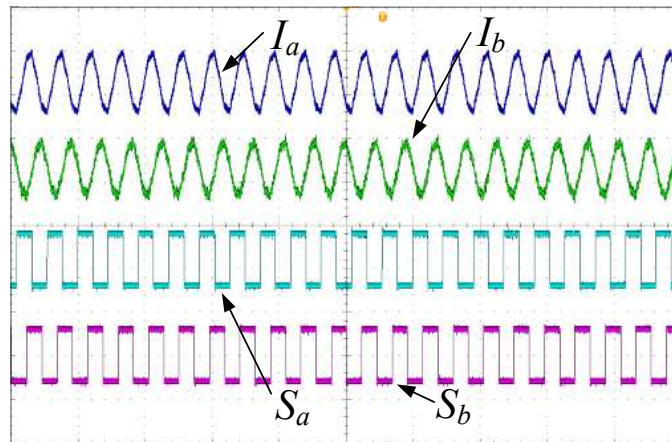
5.1.1 Experimental Results at $f_s = 8kHz$ & $f_1 = 1100Hz$

Figure 5.3 compares the phase currents I_a and I_b , and switching signals S_a and S_b before and after implementing the low frequency harmonic reduction algorithm. Figure 5.3(a) shows the current waveforms and signals when the fundamental frequency is 1100 Hz before applying the algorithm. The asymmetric pulse width of the switching signals cause a low frequency oscillation in the phase current. Figure 5.3(b) shows the waveforms after implementing the low frequency harmonic reduction algorithm. It can be observed that the turn-on time and turn-off time of each switch are balanced in one fundamental cycle. The inductances of the three phases are not perfectly balanced for the RL load used in the experimental testing. Therefore, the magnitudes of the phase A current and phase B current are not exactly equal to each other.

Figure 5.4 illustrates the spectrum analysis results of the phase current I_a



(a) I_a , I_b and S_a , S_b at $f_1=1100$ Hz before applying low frequency oscillation reduction algorithm (x-axis: 2 ms/div, y-axis: 5 A/div)



(b) I_a , I_b and S_a , S_b at $f_1=1100$ Hz after applying low frequency oscillation reduction algorithm (x-axis: 2 ms/div, y-axis: 5 A/div)

Figure 5.3: Experimental results: currents of Phase A and B before and after applying low frequency harmonic reduction algorithm

before and after applying the proposed control algorithm. The 100-Hz and 300-Hz harmonic components are significantly reduced from 0.1 p.u. to 0.0007 p.u and 0.27 p.u. to 0.012 p.u.

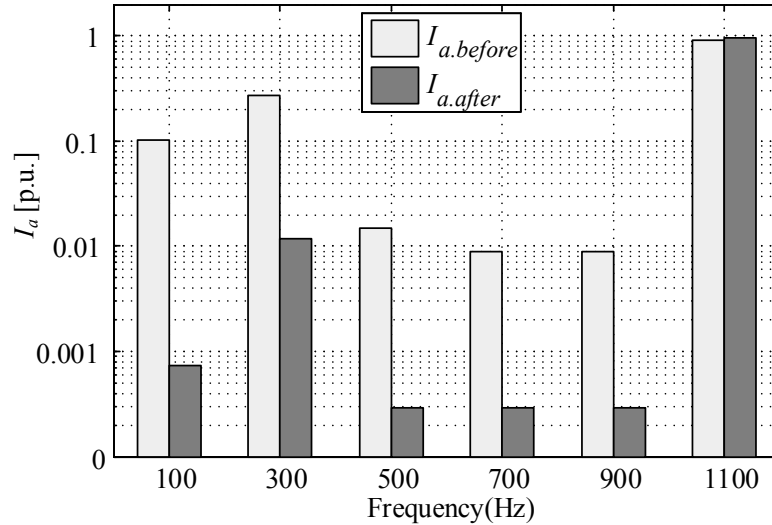
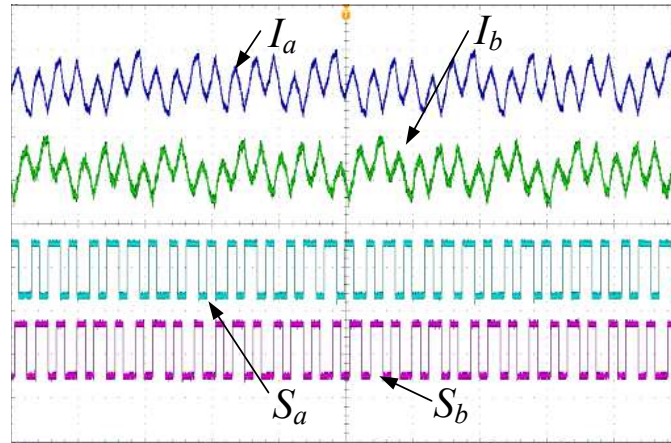


Figure 5.4: Experimental results: spectrum analysis of Phase A current before and after applying low frequency harmonic reduction algorithm

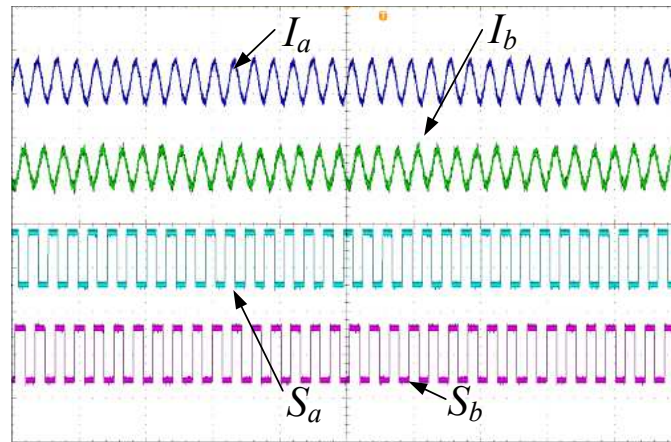
5.1.2 Experimental Results at $f_s = 8kHz$ & $f_1 = 1700Hz$

Figure 5.5 compares the phase currents I_a and I_b , and switching signals S_a and S_b before and after implementing the low frequency harmonic reduction algorithm. Figure 5.5(a) shows the current waveforms and signals when the fundamental frequency is 1700 Hz before applying the algorithm. The asymmetric pulse width of the switching signals cause a low frequency oscillation in the phase current. Figure 5.5(b) shows the waveforms after implementing the low frequency harmonic reduction algorithm. It can be observed that the turn-on time and turn-off time of each switch are balanced in one fundamental cycle.

Figure 5.6 shows the spectrum analysis results of the phase A current before and after applying the proposed algorithm. The major harmonic components with lower frequencies than the fundamental component are 100 Hz, 300 Hz, 500 Hz,



(a) I_a , I_b and S_a , S_b at $f_1=1700$ Hz before applying low frequency oscillation reduction algorithm (x-axis: 2 ms/div, y-axis: 5 A/div)



(b) I_a , I_b and S_a , S_b at $f_1=1700$ Hz after applying low frequency oscillation reduction algorithm (x-axis: 2 ms/div, y-axis: 5 A/div)

Figure 5.5: Experimental results: currents of Phase A and B before and after applying low frequency harmonic reduction algorithm

and 900 Hz. The magnitudes of the four components reduce from 0.087, 0.17, 0.52, 0.087 (all in p.u.) to 0.0004, 0.0004, 0.043, 0.0004 (all in p.u.) after the low frequency harmonic reduction algorithm is applied.

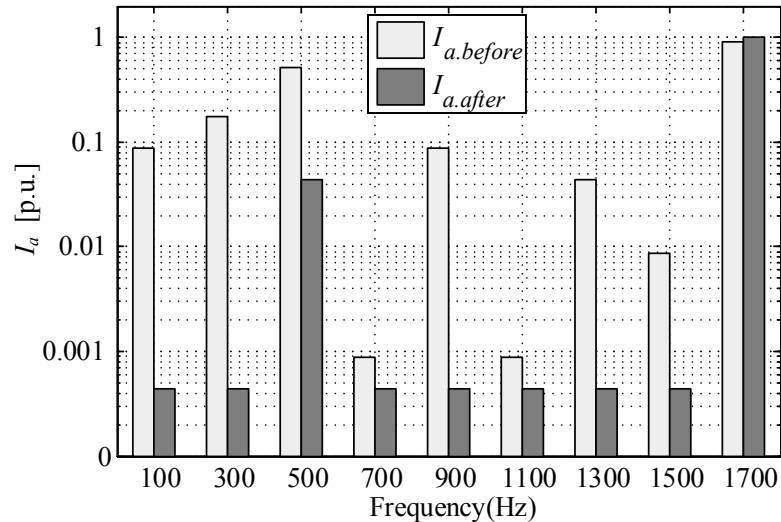


Figure 5.6: Experimental results: spectrum analysis of Phase A current before and after applying low frequency harmonic reduction algorithm

5.2 Experimental Results using Interior Permanent Magnet Synchronous Machine Load

Experimental testing using an interior permanent magnet synchronous machine has been conducted as well to verify the proposed low frequency harmonic reduction algorithm. The machine parameters are presented in Table I. The input dc voltage of the three-phase inverter was 130 V. A Texas Instrument digital signal processor TMS320F28335 was used to implement the control algorithm.

Similar to the experimental testing of the RL load, two different carrier-fundamental frequency ratios were selected in testing by using the machine load. For the first case, the machine command speed was 3030 rpm and the electrical fundamental frequency was 202 Hz. The switching frequency of 4 kHz was selected to pro-

duce non-integer carrier-fundamental ratios. For the second case, the switching frequency was 6 kHz and the machine was running at 3150 rpm.

Figure 5.7 demonstrate phase currents I_a and I_b and line-to-line voltage V_{ab} for two different switching frequencies, i.e., 4 kHz and 6 kHz. The carrier-fundamental ratio is 19.8. Figure 5.7(b) shows the same waveforms for a different switching frequency which is 6 kHz and the machine runs at about 3150 rpm. The carrier-fundamental ratio is 28.57.

Figure 5.8 shows the phase current I_a and I_b , and line-to-line voltage after implementing the low frequency harmonic reduction algorithm when the machine runs at 3030 RPM and 3150 RPM. The low frequency components of phase A and phase B current are eliminated and the line-to-line voltage V_{ab} are balanced in both two cases. In addition, the phase B current lags phase A current 120° .

Figure 5.9(a) demonstrates the spectrum analysis results of the Phase A current before and after applying the low frequency harmonic reduction algorithm when the machine runs at 3030 RPM in the first case. The sampling frequency of the measurements of the oscilloscope for the phase A current in both cases is 10 kHz. The x -axis is the frequency, which covers from 0 Hz to 3000 Hz. In addition, the y -axis is the time and the color bar represents the distribution of the power density of the phase A current. The unit of the power density in the figure is dB/Hz. Red or brighter color represents higher power density, while blue or darker color characterizes lower power density. The top figure shows the power density distribution of the phase A current before applying the reduction algorithm. Components distributed in between 0 to 200 Hz are in red color. Therefore, it

clearly shows the abundant harmonic components with lower frequencies than the fundamental frequency.

After applying the reduction algorithm, only the fundamental frequency components and 5th, 7th, 11th and 13th harmonic components are significant in the figure, which is a signature of six step control. Figure 5.9(b) demonstrates the spectrum analysis results of the Phase A current before and after applying the low frequency harmonic reduction algorithm when the machine runs at 3150 RPM. The electrical fundamental frequency is 210 Hz. After applying the reduction algorithm, low frequency harmonic components other than 5th, 7th, 11th and 13th harmonics are reduced significantly.

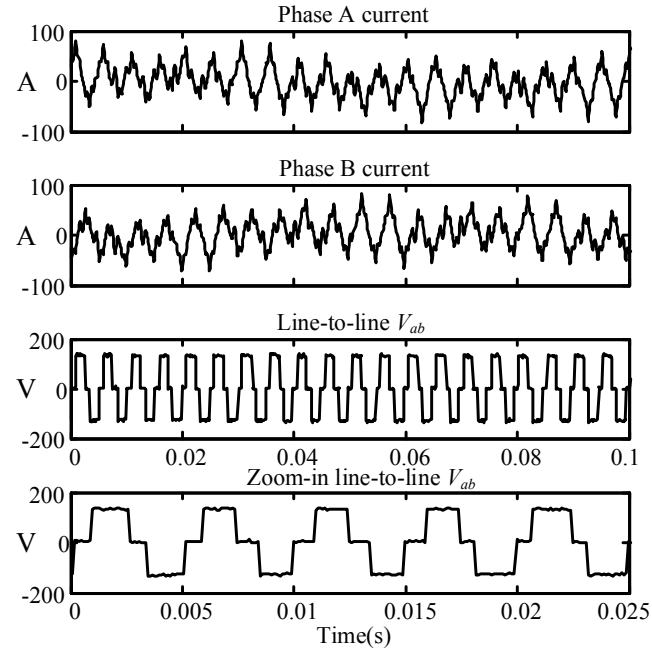
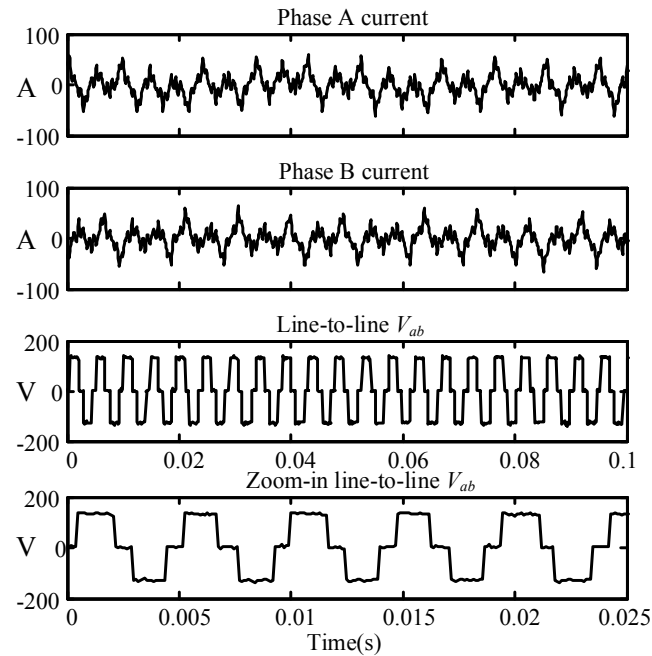
(a) $f_s=4$ kHz at 3030RPM(b) $f_s=6$ kHz at 3150RPM

Figure 5.7: Experimental results: Phase currents I_a & I_b , line-to-line voltage V_{ab} , and zoom-in line-to-line voltage V_{ab} before applying the low frequency harmonic reduction algorithm

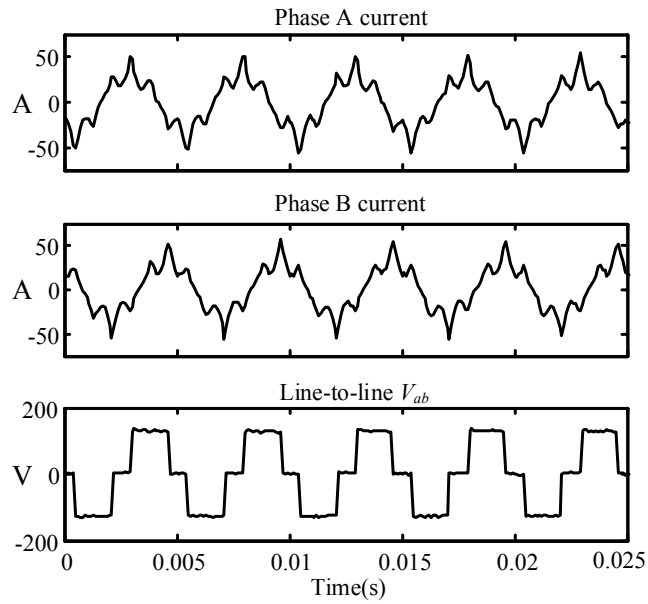
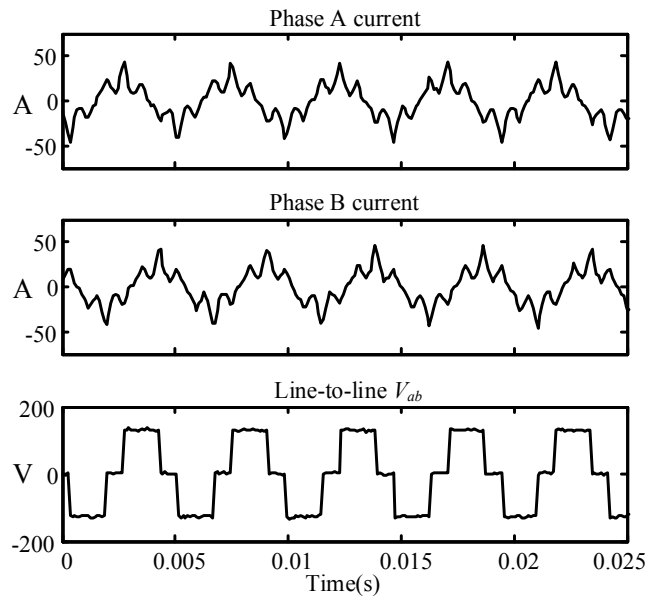
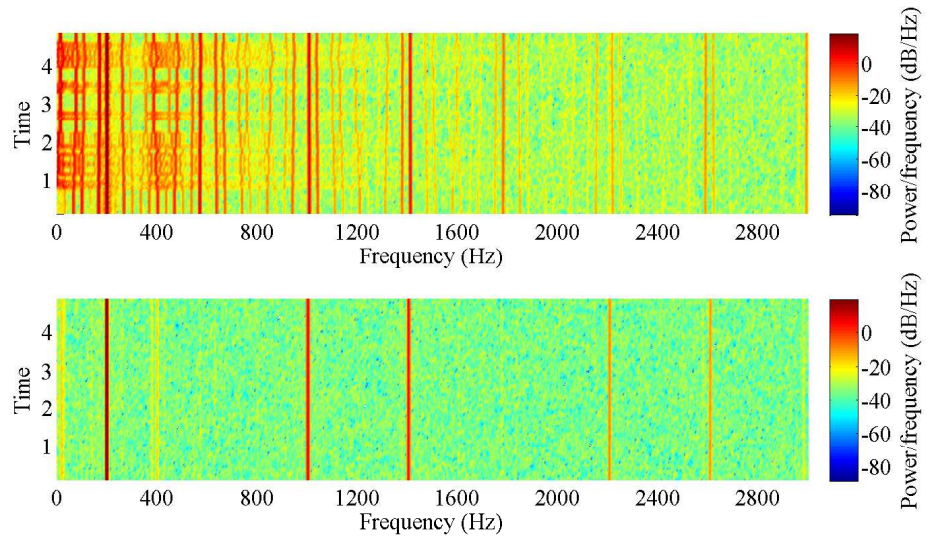
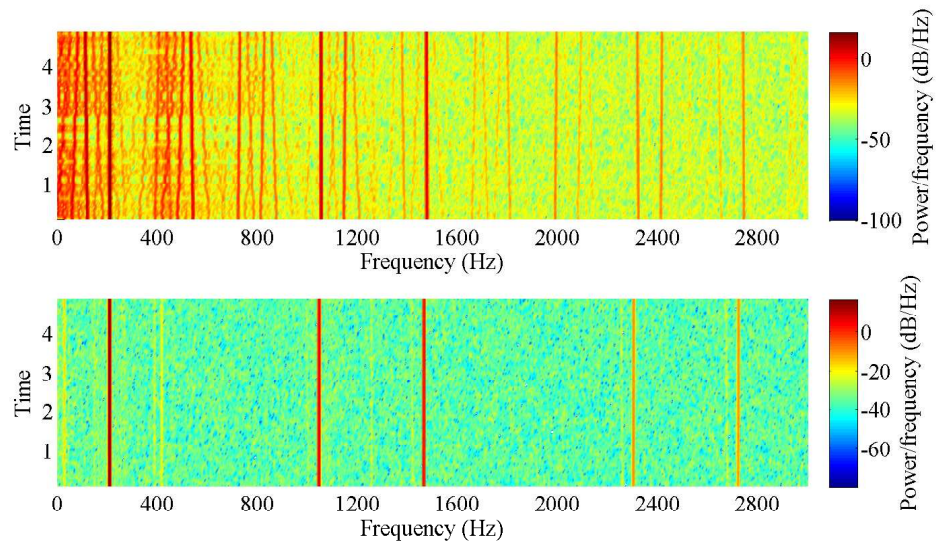
(a) $f_s=4$ kHz at 3030RPM(b) $f_s=6$ kHz at 3150RPM

Figure 5.8: Experimental results: Phase currents I_a & I_b , line-to-line voltage V_{ab} , and zoom-in line-to-line voltage V_{ab} after applying the low frequency harmonic reduction algorithm



(a) Spectrum analysis of phase current I_a at 3030 RPM



(b) Spectrum analysis of phase current I_a at 3150 RPM

Figure 5.9: Spectrum analysis of Phase A current before and after applying low frequency harmonic reduction algorithm

Chapter 6: Conclusions and Future Work

6.1 Summary and Conclusions

The major motivations of this work are to develop a new control algorithm to reduce the low frequency oscillation phase current for the six step operation of a three-phase inverter. This research work studies the low frequency harmonic current phenomenon of the three-phase inverter when it is operating in the six step control mode using a digital microcontroller. PWM algorithm in digital implementation, mathematical modeling and control algorithms of a PM synchronous machine are also introduced. Both simulations and experiment verify the proposed control algorithm and the low frequency oscillation components in the phase currents are reduced by more than 90%.

For the six step operation, the inverter switches are desired to turn on and turn off exactly at the voltage zero crossing points. In the digital implementation, the sampling and control are updated at a fixed frequency. If the voltage zero crossing point is in between two sampling points, the turn-on and turn-off events will be delayed by a period of time which is smaller than one sampling period. This delay will make the turn-on time of the top switch not equal to the turn-on time of the bottom switch over one fundamental cycle, hence create a DC offset in the output voltage and the low frequency oscillation in the phase current. This effect

is negligible if the carrier-fundamental frequency ratio is high. With decreasing carrier-fundamental frequency ratio, the magnitude of the lower frequency current oscillation is increasing and can cause many issues in the system including higher copper losses in the source and load, higher core loss in the permanent magnets on the rotor if the load is a PM machine.

This research investigates a new control method to reduce the low frequency oscillation current for the six step operation of a three-phase inverter with non-integer carrier-fundamental frequency ratios m_f . The method detects a voltage polarity change and calculates an accurate duty ratio of switches so they can be turned on and off exactly at the voltage zero crossing points. The control algorithm has two cases including that the command voltage goes from positive to negative and from negative to positive. After implementing the proposed algorithm, the positive half cycle is equal to the negative half cycle of the switching signals for each phase over one fundamental cycle. In addition, the three-phase voltage becomes balanced and the phase shifts are 120° apart. Therefore, the low frequency oscillation in the phase current is significantly reduced. Simulations and experiments are both performed to verify the algorithm using a three-phase RL load and an interior permanent magnet synchronous machine. The experiment results demonstrate a 90% reduction of the low frequency current oscillation.

6.2 Future Work

In machine drive systems, the power converter delivers the voltage based on the different control strategies [28, 32, 33]. The maximum phase voltage magnitude is $\frac{1}{2}V_{dc}$ when the inverter is controlled by the conventional sinusoidal PWM modulation. With the SVPWM modulation, the voltage magnitude will be raised up to $\frac{1}{\sqrt{3}}V_{dc}$. In addition, the magnitude will be as high as $\frac{2}{\pi}V_{dc}$ in six-step operation. The modulation index (MI) is defined as follows:

$$MI = \frac{V_s}{\frac{2}{\pi}V_{dc}} \quad (6.1)$$

where the denominator is the maximum value of the fundamental component of the phase voltage in six-step operation. Therefore, in SVPWM modulation, the linear modulation region is $MI \leq \frac{\frac{1}{\sqrt{3}}}{\frac{2}{\pi}} = 0.907$. When the modulation is beyond 0.907, SVPWM inverter operates in non-linear or over-modulation region. If the control method of the inverter jump from SVPWM to Six-step directly, the modulation will increase from 0.907 to 1 dramatically, which causes over-current in each phase. Smooth transition means the modulation index increases from 0.907 to 1 gradually in over-modulation region [34]. In order to reduce the over-current performance during the transient, smooth transition control algorithm is needed.

In this thesis, steady-state performance of phase currents and voltages in six-step operation are investigated. In physical testing, the machine is started up by using PWM control. After the PM machine reaches in steady-state and the modulation index is near saturation, the control is switched from PWM to Six-

step directly. The transition causes overshooting in phase currents. Therefore, smooth transition without significant phase current overshooting is considered as future research work.

Bibliography

- [1] D. Ludois and G. Venkataramanan, “An Examination of AC/HVDC Power Circuits for Interconnecting Bulk Wind Generation with the Electric Grid,” *Energies*, vol. 3, pp. 1263–1289, 2010.
- [2] J. K. Reed, “Topology, modeling and analysis of bridge of bridge dc-ac and ac-dc power converters,” Master’s thesis, University of Wisconsin-Madison, 2014.
- [3] N. Limsuwan, “Field intensifying interior permanent magnet synchronous machines for power conversion and self-sensing control,” Master’s thesis, University of Wisconsin-Madison, 2009.
- [4] Y. Zhang, “Sensorless vector control and field weakening operation of permanent magnet synchronous machines,” Ph.D. dissertation, The Ohio State University, 2010.
- [5] C. Zwyssig, J.W. Kolar and S.D. Round, “Megaspeed Drive Systems: Pushing Beyond 1 Million r/min,” *IEEE/ASME Trans. Mechatronics*, vol. 14, no. 5, pp. 564–574, Apr, 2009.
- [6] I. Ralev, T. Lange and R. De Doncker, “Wide Speed Range Six-Step Mode Operation of IPMSM Drives with Adjustable DC-link Voltage,” in *International Conference on Electrical Machines and Systems (ICEMS)*, Hangzhou, China, Oct, 2014, pp. 2987–2993.
- [7] Y. Kwon, S. Kim and S. Sul, “Six-Step Operation of PMSM With Instantaneous Current Control,” *IEEE Trans. Industry Application*, vol. 50, no. 4, pp. 2614–2624, Jul/Aug, 2014.
- [8] D.C. Rus, N.S. Preda, I.I. Incze, M. Imecs and C. Szabo, “Comparative Analysis of PWM Techniques: Simulation and DSP Implementation,” in *IEEE International Conference on Automation Quality and Testing Robotics (AQTR)*, Cluj-Napoca, May, 2010, pp. 1–6.

- [9] P. Stumpf, R.K. Jordan and I. Nagy, "Comparison of Naturally Sampled PWM Techniques in Ultrahigh Speed Drives," in *IEEE International Symposium on Industrial Electronics (ISIE)*, Hangzhou, China, May, 2012, pp. 246–251.
- [10] G.R. Walker, "Digitally-implemented Naturally Sampled PWM Suitable for Multilevel Converter Control," *IEEE Trans. Power Electronics*, vol. 18, no. 6, pp. 1322–1329, Nov, 2003.
- [11] Z. Chen, H. Mao, X. Yang and Z. Wang, "A Study on Pulse Width Errors of Digitized Naturally Sampled PWM," in *IEEE Power Electronics Specialists Conference*, Rhodes, Greece, Jun, 2008, pp. 592–597.
- [12] P. Stumpf, R.K. Jordan and I. Nagy, "DC Components and Subharmonics Generated by Naturally Sampled PWM Techniques," in *IECON Annual Conference on IEEE Industrial Electronics Society*, Montreal, QC, Oct, 2012, pp. 327–332.
- [13] A.M. Rahimi, A. Khaligh and A. Emadi, "Sub-Harmonic Problem in Multi-Converter Vehicular Power Systems," in *IEEE Vehicle Power and Propulsion Conference*, Windsor, CO, Sept, 2006, pp. 1–5.
- [14] P. Stumpf, R.K. Jordan and I. Nagy, "Subharmonics Generated by Space Vector Modulation in Ultrahigh Speed Drives," *IEEE Transactions on Industrial Electronics*, vol. 59, no. 2, pp. 1029–1037, May, 2011.
- [15] R. K. Jordan, P. Stumpf, P. Bartal, Z. Varga and I. Nagy, "A Novel Approach in Studying the Effects of Subharmonics on Ultrahigh-Speed AC Motor Drives," *IEEE Trans. Industrial Electronics*, vol. 58, no. 4, pp. 1274–1281, Apr, 2011.
- [16] S. Halasz, "Discontinuous Carrier-Based PWM With Low Switching Frequency," in *IEEE International Power Electronics and Motion Control Conference and Exposition*, Antalya, Turkey, Sept, 2014, pp. 778–786.
- [17] S. Halasz, "DC Components and Subharmonics of Carrier-Based PWM," in *IEEE International Power Electronics and Motion Control Conference*, Novi Sad, Serbia, Sept, 2012, pp. 1–7.

- [18] M. Bierhoff and F. W. Fuchs, "DC Link Harmonics of Three Phase Voltage Source Converters Influenced by the Pulse Width Modulation Strategy- an Analysis," in *IEEE Industrial Electronics Society*, Nov, 2005, pp. 491–496.
- [19] J. Holtz, W. Lotzkat, and A. M. Khambadkone, "On continuous control of PWM inverters in the overmodulation range including the six-step mode," *IEEE Transactions on Power Electronics*, vol. 8, no. 4, pp. 546–553, Oct, 1993.
- [20] R. J. Kerkman, D. Leggate, B. J. Seibel, and T. M. Rowan, "Operation of PWM voltage source-inverters in the overmodulation region," *IEEE Transactions on Industrial Electronics*, vol. 43, no. 1, pp. 132–141, Feb, 1996.
- [21] Z. Peroutka and T. Glasberger, "Comparison of methods for continuous transition of space vector PWM into six-step mode," in *EPE International Power Electronics and Motion Control Conference*, Portoroz, Slovenia, Aug, 2006, pp. 925–930.
- [22] A. Jidin, N. Idris, A. H. M. Yatim, and M. Elbuluk, "A novel overmodulation and field weakening strategy for direct torque control of induction machines," in *IEEE Industry Applications Society Annual Meeting*, Edmonton, Alta. Canada, Oct, 2008.
- [23] Y. Inoue, Y. Maeda, S. Morimoto, and M. Sanada, "Square-wave operation of direct torque controlled PMSM drive system," in *IEEE Energy Conversion Congress and Exposition*, Denver, CO, Sep, 2013, pp. 1801–1807.
- [24] H.W. Van Der Broeck, H. Skudelny and G.V. Stanke, "Analysis and Realization of a Pulsewidth Modulator Based on Voltage Space Vectors," *IEEE Trans. Industry Application*, vol. 24, no. 1, pp. 142–150, Jan/Feb, 1988.
- [25] M.S. Balakrishnan and R. Theagarajan, "High Frequency Carrier Digital PWM for Non-Sinusoidal Modulating Waveforms," in *International Conference on Business, Engineering and Industrial Applications (ICBEIA)*, Kuala Lumpur, Malaysia, Jun, 2011, pp. 57–61.
- [26] W.V. Lyon, "Transient Conditions in Electric Machinery," *Transactions of the American Institute of Electrical Engineers*, vol. 42, no. 4, pp. 388–407, Apr, 1923.

- [27] H. Nakai, H. Ohtani, E. Satoh and Y. Inaguma, "Development and Testing of the Torque Control for the Permanent-Magnet Synchronous Motor," *IEEE trans. Industrial Electronics*, vol. 52, no. 3, pp. 800–806, Jun, 2005.
- [28] T. Schoenen, A. Krings, D. van Treek and R. W. De Doncker, "Maximum DC-Link Voltage Utilization for Optimal Operation of IPMSM," in *Electric Machines and Drives Conference*, Miami, IL, May, 2009, pp. 1547–1550.
- [29] Y. Zhang, F. Lin, Z. Zhang and L. Xu, "Direct Voltage Control for Field Weakening Operation of PM Machines," in *Power and Energy Conference at Illinois*, Urbana-Champaign, IL, Feb, 2010, pp. 20–24.
- [30] R. Monajemy and R. Krishnan, "Performance Comparison for Six-Step Voltage and Constant back EMF Control Strategies for PMSM," in *Industry Applications Conference*, Phoenix, AZ, May, 1999, pp. 165–172.
- [31] L. Cohen, "Time-frequency distributions-A review," *Proc. IEEE*, vol. 77, no. 7, pp. 941–981, Jul, 1989.
- [32] M. Aravind and T. Bhattacharya, "FPGA Based Synchronized Sinusoidal Pulse Width Modulation with Smooth Transition into Overmodulation and Six Step Modes of Operation for Three Phase AC Motor Drives," in *IEEE International Conference on Power Electronics, Drives and Energy Systems*, Bengaluru, India, Dec, 2012, pp. 1–6.
- [33] A. Tripathi, B. Dwivedi and D. Chandra, "A Novel Approach Towards Six-step Operation in Overmodulation Region in SVPWM VSI," *ARPJN Journal of Engineering and Applied Sciences*, vol. 3, no. 5, pp. 8–12, Oct, 2008.
- [34] A. M. Khambadkone and J. Holtz, "Compensated Synchronous PI Current Controller in Overmodulation Range and Six-Step Operation of Space-Vector-Modulation-Based Vector-Controlled Drives," *IEEE Trans. Industrial Electronics*, vol. 49, no. 3, pp. 574–580, Jun, 2002.

